Computational and Data-Enabled Analysis for Sustainable Transportation Systems

The Pennsylvania State University
University of Maryland
University of Virginia
Virginia Polytechnic Institute & State University
West Virginia University

The Pennsylvania State University
The Thomas D. Larson Pennsylvania Transportation Institute
Transportation Research Building ❖ University Park, PA 16802-4710
Phone: 814-863-5621 ❖ Fax: 814-863-3707

1. Report No. PSU-2011-06	2. Government Accession No.	3. Recipient's Catalog No.
4. Title and Subtitle Computational and Data-Enabled Analysis for Sustainable Transportation Systems		**5. Report Date** Oct. 30, 2014 **6. Performing Organization Code** MAUTC Project No. PSU2011-06
7. Author(s) Tao Yao and Terry Friesz		**8. Performing Organization Report** LTI 2015-06
9. Performing Organization Name and Address The Thomas D. Larson Pennsylvania Transportation Institute The Pennsylvania State University 201 Transportation Research Building University Park, PA, 16802-4710		**10. Work Unit No. (TRAIS)** **11. Contract or Grant No.** DTRT 07-G-0003
12. Sponsoring Agency Name and Address US Department of Transportation Research & Innovative Technology Admininstration UTC Program, RDT-30 1200 New Jersey Ave., SE Washington, DC 20590		**13. Type of Report and Period Covered** Final Report 9/1/2011-1/31/2013 **14. Sponsoring Agency Code**

15. Supplementary Notes

16. Abstract

Transportation planners and traffic engineers are faced nowadays with immense modeling challenges arising from several emerging policy, planning, and engineering developments. In fact, the recent emergence of mobile sensing and traffic monitoring technology has provided an unprecedented amount of information and data for traffic analysis, demanding the adaptation of mathematical and physical models to a new generation of cyberinfrastructure. Some of the major challenges that traffic models meet include: computational tractability, very large-scale deployment, real-time application decision support, multiple time scales, and fusion of dissimilar data. This research takes a major step in developing analytical, holistic mathematical models and traffic analysis tools capable of addressing data-enabled traffic modeling, estimation, control and optimization problems, leading to a more efficient, reliable, and sustainable transportation system. In the project, we constructed: (1) a class of Mathematical Programming with Equilibrium Constraints (MPEC) problems to understand and mitigate congestion externalities and mobile source emissions, and (2) a class of Mixed Binary Integer Programs (MBIPs) for data fusing, real-time traffic estimation and prediction, as well as data-enabled traffic control.

17. Key Words	18. Distribution Statement
Mathematical Programming with Equilibrium Constraints, Mobile Source Emissions, Mixed Binary Integer Program	No restrictions. This document is available from the National Technical Information Service, Springfield, VA 22161

19. Security Classif. (of this report)	20. Security Classif. (of this page)	21. No. of Pages	22. Price
Unclassified	Unclassified	33	

Table of Contents

Computational and Data Enabled Analysis for Sustainable Transportation Systems

FINAL REPORT

January 31, 2013

By Tao Yao (PI)

Terry Friesz (Co-PI)

1. Report No. PSU-2011-06	2. Government Accession No.	3. Recipient's Catalog No.
4. Title and Subtitle Computational and Data-Enabled Analysis for Sustainable Transportation Systems		**5. Report Date** Oct. 30, 2014 **6. Performing Organization Code** MAUTC Project No. PSU2011-06
7. Author(s) Tao Yao and Terry Friesz		**8. Performing Organization Report** LTI 2015-06
9. Performing Organization Name and Address The Thomas D. Larson Pennsylvania Transportation Institute The Pennsylvania State University 201 Transportation Research Building University Park, PA, 16802-4710		**10. Work Unit No. (TRAIS)** **11. Contract or Grant No.** DTRT 07-G-0003
12. Sponsoring Agency Name and Address US Department of Transportation Research & Innovative Technology Admininstration UTC Program, RDT-30 1200 New Jersey Ave., SE Washington, DC 20590		**13. Type of Report and Period Covered** Final Report 9/1/2011-1/31/2013 **14. Sponsoring Agency Code**

15. Supplementary Notes

16. Abstract

Transportation planners and traffic engineers are faced nowadays with immense modeling challenges arising from several emerging policy, planning, and engineering developments. In fact, the recent emergence of mobile sensing and traffic monitoring technology has provided an unprecedented amount of information and data for traffic analysis, demanding the adaptation of mathematical and physical models to a new generation of cyberinfrastructure. Some of the major challenges that traffic models meet include: computational tractability, very large-scale deployment, real-time application decision support, multiple time scales, and fusion of dissimilar data. This research takes a major step in developing analytical, holistic mathematical models and traffic analysis tools capable of addressing data-enabled traffic modeling, estimation, control and optimization problems, leading to a more efficient, reliable, and sustainable transportation system. In the project, we constructed: (1) a class of Mathematical Programming with Equilibrium Constraints (MPEC) problems to understand and mitigate congestion externalities and mobile source emissions, and (2) a class of Mixed Binary Integer Programs (MBIPs) for data fusing, real-time traffic estimation and prediction, as well as data-enabled traffic control.

17. Key Words	18. Distribution Statement
Mathematical Programming with Equilibrium Constraints, Mobile Source Emissions, Mixed Binary Integer Program	No restrictions. This document is available from the National Technical Information Service, Springfield, VA 22161

19. Security Classif. (of this report)	20. Security Classif. (of this page)	21. No. of Pages	22. Price
Unclassified	Unclassified	33	

1 Introduction

According to the U.S. Environmental Protection Agency (2006), in 2003, the transportation sector contributed 27 percent of total U.S. greenhouse gas (GHG) emissions. This number is expected to grow rapidly with an estimated 48 percent increase in transportation energy use by 2015. Future transportation service network designs ought to take into account environmental and sustainability issues. In view of these issues, the project proposed two models that seek to improve the sustainability of a transportation system: (1) an mixed-integer linear programming model for adaptive signal control that constrains the emission rate on each link of a traffic subnetwork, and (2) a dynamic second-best congestion toll problem with embedded emission model for the management and control of tollable vehicular networks.

1.1 Traffic signal control with emission constraints

Traffic signals are essential elements in the management of transportation networks. Over the past decades, signal control strategies have evolved greatly, from simple, fixed-time plans based on historical data and updated infrequently throughout the day to adaptive control systems that update continuously in response to real-time traffic information. The performance of a signal control system depends on two primary factors: the optimization procedure employed and the objective of the optimization.

1.1.1 Mathematical programming approach to traffic signal control

We distinguish between two optimization procedures: (1) heuristic approaches, such as those developed with feedback control, genetic algorithms, and fuzzy logic; and (2) exact approaches, such as those arising from mathematical control theory and mathematical programming. Among these exact approaches, *mixed-integer programs* (MIPs) are of particular interest and have been used extensively in the signal control literature. For example, Improta and Cantarella (1984) formulated and solved the traffic signal control problem for a single road junction as a mixed binary integer program. Lo (1999a,b) employed the *cell transmission model* (CTM) (Daganzo, 1994; 1995) and casted a signal control problem as a mixed-integer linear program. In these projects, the authors were able to address time-varying traffic patterns by adopting dynamic signal timing plans. Lin and Wang (2004) applied the same formulation based on CTM to capture more realistic features of signalized junctions such as the total number of vehicle stops and signal preemption in the presence of emergency vehicles.

One subtle issue associated with CTM-based mathematical programs is the phenomenon known as traffic holding, which stems from the linear relaxation of the nonlinear dynamic. Such an action induces the unintended holding of vehicles, i.e., a vehicle is held at a cell even though there is capacity available downstream for the vehicle to advance. The traffic holding can be avoided by introducing additional binary variables (See Lo, 1999c). However, this approach ends up with a significant amount of binary variables and yields the program computationally demanding. An alternative way to treat the holding problem is to manipulate the objective function such that the optimization mechanism enforces the full utilization of available capacities in the network. This approach, however, strongly depends on specific structure of the problem and the underlying optimization procedure. A more in-depth discussion on traffic holding can be found in Shen et al. (2007).

This project is concerned with controlling signalized junctions where the dynamics of vehicular flows are governed by the network extension of the Lighthill-Whitham-Richards model. In particular, we employ the *link-based kinematic wave model* (LKWM) proposed by Han et al. (2012). This

model describes network dynamics with variables associated to the entrance and exit of each link. It employs a Newell-type variational argument Newell (1993); Daganzo (2005) to capture shock waves and vehicle spillback. Analytical properties of this model pertaining to solution existence, uniqueness, and well-posedness are provided by Han et al. (2012). A discrete-time version of the LKWM, known as the *link transmission model*, was discussed by Yperman et al. (2005). In contrast to the cell-based math programming approaches, where the variables of interest correspond to each cell and each time interval, the model proposed in this project is link-based (i.e., the variables are associated with each link and each time interval). The resulting MILP substantially reduces the number of (binary) variables needed to properly carry out the flow dynamics. In addition, the link-based approach prevents vehicle holding within a link without resorting to the use of many binary variables. The formulation proposed also captures key phenomena of vehicular flow at junctions in urban networks, such as the formation, propagation, and dissipation of physical queues, vehicular spillback, and vehicle turning at intersections. It also considers important features of signal control such as dynamic signal timing plans and time-varying flow patterns.

1.1.2 Recent advancement in solving MILP

Due to the critical role of an MILP in mathematical programming, the solution schemes for an MILP have been heavily investigated in literature (see Bernhart et al., 1998, and Geoffrion and Marstern, 1972, for reviews on MILP). Despite the presence of integer variables, The computational and algorithmic advances in the last decade have made an MILP of larger problem scales fairly efficiently computable Bertsimas et al. (2011) via highly commercialized solvers, including CPLEX and Gurobi, given that linearity is maintained in both objective and constraints. However, for the nonlinear case, even though some mixed-integer quadratic programs can be handled by both CPLEX and Gurobi, nonlinearity will result in a substantial increase in computational overhead in general. If, in addition, any of the objective and/or constraint functions become nonconvex, the problem will become extremely challenging to solve, or, sometimes, even to identify a feasible solution Burer and Letchford (2012).

1.1.3 Considering vehicle emissions in the optimization procedure

The majority of adaptive traffic signal control schemes update signal timings to minimize total vehicular delays. Representatives of such signal-control systems are OPAC (Gartner, 1983), RHODES (Mirchandani and Head, 2000), SCAT (Sims and Dobinson, 1980) and SCOOT (Hunt et al., 1982). Other control strategies seek to minimize delays to a subset of vehicles; for example, the goal of transit signal priority strategies is to reduce delays for transit vehicles, often to the detriment of those remaining; for more details, see Skabardonis (2000). More recently, a transit signal priority strategy was proposed to minimize total person delay, which essentially considers a weighted average of vehicular delay using the passenger occupancies of each vehicle as the weights Christofa et al. (2013).

Relatively less attention has been given to vehicular emissions when optimizing signal timings. The earliest work appears to be by Robertson et al. (1980), but this work used macroscopic simulations that did not accurately account for vehicle dynamics at intersections. The efforts that followed either relied on combining detailed emissions models with outputs from microscopic simulations or models (Stevanovic et al., 2009; Li and Shimamoto, 2011; Lin et al., 2010; Lv et al., 2013), or they relied on macroscopic emissions models estimated from data (Aziz and Ukkusuri, 2012; Zhang et al., 2013). The former approach is more accurate and relies on simulation-based optimization that requires significant computational effort. The latter is useful but as pointed out by a survey project (Szeto et al., 2012) and the literature therein, the environmental considerations typically result in

nonlinear and nonconvex constraints and objective functions in the mathematical programming formulation, which itself imposes a tremendous computational burden. As a result, heuristic methods, such as one found in Ferrari (1995), are developed for this type of problem. Classical methods such as the inner penalty technique Yang and Bell (1997) and augmented Lagrangian multiplier technique Yang et al. (2010) have also been used.

This project presents a novel approach to circumvent the aforementioned computational challenge by including emissions considerations and optimization constraints (e.g., maximizing throughput subject to some emissions standard) and reformulating these constraints as linear functions through the use of numerical experimentation and robust optimization. This method is made possible by leveraging observed relationships between aggregated link emission rates and the link occupancy that arise when certain macroscopic or mesoscopic emission models are employed. Such empirical observations are supported by extensive numerical simulations, as we shall demonstrate below. A detailed description of the simulation and synthetic data is presented in Section 2.2.

Despite the strong correlation between the aggregated emission rate and certain macroscopic traffic quantities (e.g., link occupancy), there are non-negligible errors associated with such approximation. Errors and perturbations to a deterministic model can render an optimal solution in the ideal case suboptimal in implementation. A natural approach to capture uncertainty is by assuming that uncertain parameters follow certain probability distributions and by employing the notions and methodologies in stochastic programming. However, such an approach has two main limitations: (1) exact knowledge of error distributions is often difficult to acquire, and (2) stochastic programming is recognized as highly intractable to solve even with linear objective function and linear constraint functions. In view of these challenges, we propose to handle uncertainty in the perspective of robust optimization.

A robust optimization is a distribution-free uncertainty set approach that seeks to minimize the worst-case cost and/or to remain feasible in the worst scenario. Compared to stochastic programming, robust optimization makes no assumption on the underlying distribution of uncertain parameters. Moreover, it has been shown to work as a powerful approximation to stochastic programming and even probabilistic models with significantly reduced computational cost (Ben-Tal and Nemirovski, 1998, 1999, 2000; Bertsimas et al., 2011a,b; Bandi and Bertismas, 2012; Rikun, 2011). Although solutions to robust optimization problems can be relatively conservative, the conservatism is adjustable with the flexibility of choosing uncertainty sets (Bertsimas and Sim, 2004). A comprehensive review of robust optimization is provided by Bertsimas et al. (2011a).

1.1.4 Contributions

In this project, we will invoke the robust optimization approach to capture the errors arising from statistical learning of the emission model. The goal of this approach is to maximize the total throughput of the signalized network while keeping the vehicle emission below a desired level, even in the worst case. The complex nonlinear and nonconvex signal optimization problem with emissions will be reformulated as a *mixed-integer linear program* (MILP) in most cases, which can be efficiently solved using most commercial software packages. The proposed MILP captures vehicle spillbacks, features time-varying signal cycle lengths and splits, avoids the traffic holding problem, and addresses nonconvex emissions constraints in a mathematically tractable way. The proposed solution method is tested using a synthetic experiment to demonstrate its performance.

1.2 Bi-objective dynamic congestion toll pricing model

In this project, we propose a dynamic second-best congestion toll problem with embedded emission model for the management and control of tollable vehicular networks. We assume that users of a

given network are selfishly minimizing their own disutility, which consists of travel delay, early/late arrival penalties as well as the price of tolls. On top of that, there exists a central authority that undertakes the role of the Stackelberg leader, whose objective includes two different aspects: the network efficiency and the environmental well-being in the presence of vehicle-driven emission.

The upper-level decision variable for the central authority (Stackelberg leader) is a dynamic congestion toll imposed on certain links of the network, while the lower-level decision variables for the travelers (Stackelberg follower) include route and departure time choices. The proposed congestion pricing problem with embedded emission model is formulated as a *mathematical programming with equilibrium constraints* (MPEC) problem, with multiple objectives including the mitigation of both congestion and traffic emission on a network-wide level.

To solve the multi-objective MPEC problem, we start by rewriting the *differential variational inequality* (DVI) formulation of dynamic user equilibrium into a differential complementarity problem. Then, we employ a weighted-sum scalarization method to handle the multiple objectives. With these two steps, the multi-objective MPEC problem is transformed into a single-objective *mathematical program with complementarity constraints* (MPCC). To avoid the loss of constraint qualification, we relax the mathematical program by applying a quadratic penalty-based method. The relaxed problem is then solved with a gradient projection method mentioned by Friesz (2010).

1.2.1 Congestion toll pricing

The idea of employing toll pricing to mitigate congestion arises from the congestion pricing strategy originally proposed by Pigou (1920). In the literature, toll pricing problems can be classified into two categories: (1) first-best toll pricing, which means every arc of the network is tollable; and (2) second-best toll pricing, which assumes that only a subset of arcs is tolled for political or other reasons. Examples of the first category include marginal social cost pricing strategy Arnott and Kraus (1998), and several other models and methodologies (Hearn and Ramana, 1998; Dial, 1999, 2000). Regarding the second-best tolling strategy, Lawphongpanich and Hearn (2004) propose a *mathematical program with equilibrium constraints* (MPEC) approach to compute the optimal toll prices. All the aforementioned literature are restricted to the static case. For a comprehensive review on static road pricing problems, the reader is referred to Yang and Huang (2005). By nature of these problems, only route choices of travelers are captured by the models.

In the past two decades, *dynamic traffic assignment* (DTA) models and dynamic congestion tolling problems have received increased attention due to their capability of capturing not only route choices but also departure time choices of travelers. Dynamic congestion pricing in the presence of traffic bottlenecks have been investigated by Arnott et al. (1990), Arnott and Kraus (1998), Braid (1996), and De Palma and Lindsey (2000). Friesz et al. (2007) propose an MPEC problem and a solution approach to determine the optimal second-best tolling strategy, using the *link delay model* (LDM) original introduced by Friesz et al. (1993). Yao et al. (2012) further study a dynamic congestion pricing problem in the presence of demand uncertainty. Wismans (2012) employs the cell transmission model to study the multi-objective congestion management problem. He uses a genetic algorithm and response surface methods for solving the MPEC problems. A more complete review of existing dynamic congestion pricing models and solution approaches is presented by Yao et al. (2012).

In this study, we seek to explore the effectiveness of second-best tolling strategies in minimizing both traffic congestion and automobile-induced emissions. To this end, we propose a multi-objective MPEC problem to determine the optimal toll price. Such an MPEC model has a lower-level dynamic user equilibrium problem that employs the LWR-Lax model Friesz et al. (2013) for the *dynamic network loading* subproblem. The contribution made by this project is as follows.

- We propose an approach of embedding emission models into the *dynamic network loading* (DNL) submodel of the dynamic user equilibrium problem. Such an approach is compatible with a variety of traffic flow models and emission models, which may capture vehicle spillback, and acceleration/deceleration.
- We propose to reformulate the dynamic MPEC model into a single-level optimal control problem using the equivalence between the DVI and the complementarity systems. The reformulation admits existing solution schemes.
- A Braess-type paradox is reported in our numerical results, which extends the classical Braess paradox Braess (1969) to a dynamic case and to the context of environmental well-being. Such observation delivers further managerial insights to sustainable road network management.

1.2.2 Dynamic user equilibrium model

In this report, we employ the *simultaneous route-and-departure choice* (SRDC) dynamic user equilibrium model proposed by Friesz et al. (1993). For the SRDC notion of DUE, unit travel cost, including early and late arrival penalties, is identical for those route and departure time choices selected by travelers between a given origin-destination pair. Such a problem is articulated and formulated as a *variational inequality* (VI) by Friesz et al. (1993). The DUE model typically consists of two major components: the mathematical notion of equilibrium among Nash agents, and the network performance model known as the dynamic network loading submodel. The DNL aims at describing and predicting temporal evolution of system states by combining link dynamics and flow propagation constraints with link and path delay models. Note that, by referring to the network loading procedure, we are neither employing nor suggesting a sequential approach to the study and computation of DUE. Rather, a subset of the equations and inequalities comprising a complete DUE model may be grouped in a way that identifies a traffic assignment subproblem and a network loading subproblem. Such a grouping and choice of names is merely a matter of convenient language that avoids repetitive reference to the same mathematical expressions. Use of such language does not alter the need to solve both the assignment and loading problems consistently and, thus, simultaneously.

Friesz et al. (2001) solve the differential variational inequality formulation of DUE and the DNL subproblem simultaneously by formulating the arc dynamics, flow propagation constraints as a system of ordinary differential equations with state-dependent time lags. By doing so, they turn the DUE problem into a "single-level" DVI problem that can be handled in the optimal control framework. In addition, necessary conditions for optimal control problems with state-dependent time lags are derived therein. Friesz and Mookherjee (2006) combine the theory of optimal control and the theory of infinite dimensional VIs are combined to create an implicit fixed point algorithm for calculating DUE. Friesz et al. (2011) extend the time scale in which DUE problems are analyzed from within-day to day-to-day. A dual-time scale DUE is articulated and solved as a result. Friesz et al. (2013) consider the Lighthill-Whitham-Richards model (Lighthill and Whitham, 1955; Richards, 1956) for the DNL submodel. The authors employ a variational method, known as Lax formula (Lax, 1957; Evans, 2010), derived for scalar conservation laws and Hamilton-Jacobi equations. In that project, the DNL subproblem is formulated as a system of *differential algebraic equations* (DAEs), which can be efficiently solved for medium- and large-scale networks.

1.2.3 Automobile emission models

Modeling approaches for automobile source emission can be classified into three categories: microscopic, macroscopic, and mesoscopic approaches. The microscopic emission models are relatively

accurate: they characterize the emission rate on the level of a single vehicle, based on the physical attributes of the vehicle, driving behavior of the driver, as well as the surrounding environment. It is assumed that the emission rate $e(t)$ of a moving vehicle is to be expressed as a function of instantaneous velocity $v(t)$ and acceleration $a(t)$,

$$e(t) \;=\; f_1\big(v(t),\, a(t)\big). \tag{1.1}$$

Such models can be easily calibrated and validated in a laboratorial environment. There are several emission models based on the microscopic emission mechanism, e.g., Barth et al. (1996), Panis et al. (2006), and Rakha et al. (2004). The drawback of the microscopic modeling approach is the lack of measurements associated with each individual car on the road. On the other hand, it is relatively easy to measure the traffic dynamics on a macroscopic level. The macroscopic emission models (Ekström et al. 2004) express the average emission rate $\bar{e}(t)$ on a road segment as a function of the average density $\bar{\rho}$ and average velocity $\bar{v}(t)$ in that same segment

$$\bar{e}(t) \;=\; f_2\big(\bar{\rho}(t),\, \bar{v}(t)\big) \tag{1.2}$$

The drawback of the macroscopic modeling approaches for emission lies in the fact that the model is difficult to calibrate and validate, due to insufficient emission measurements on a road. The third type of emission models, the mesoscopic emission models, approximate individual vehicles' dynamics using macroscopic flow models and measurements. Then the macroscopic emission rate is aggregated among individual vehicles, while the emission rate of each individual vehicle is computed at a microscopic level. The mesoscopic models (Csikós et al., 2011; Csikós and Varga, 2011; Zegeye et al., 2010) take the modeling advantages of both macroscopic traffic flow models and microscopic emission models, avoiding the drawbacks of the previous two approaches. However, combining a macroscopic traffic model that ignores granularity of microscopic quantities with an accurate microscopic emission model may introduce additional uncertainties into the model. Therefore, the mesoscopic models need to be carefully calibrated and validated using macroscopic traffic and emission measurements.

In this project, the process of emission estimation is embedded in the procedure of dynamic network loading within the DUE problem. The DNL procedure also provides a basis for the comparison of various microscopic and macroscopic emission functions, among which we distinguish between the two-argument functions $e(t) = f_1\big(v(t),\, a(t)\big)$ and the single-argument functions $e(t) = f_3\big(v(t)\big)$.

The two-argument functions, such as the one proposed in the modal emission model (Barth et al., 1996), apply a physical approach that matches the power demand of a vehicle to various driving conditions including low/high speed cruising, acceleration/deceleration, idling, and stop-and-go, etc. Such models are relatively accurate and can be calibrated for different types of vehicles. However, it is relatively difficult to integrate the modal model into a macroscopic traffic flow model. In particular, the higher order traffic quantities such as acceleration/deceleration cannot be sufficiently captured by first-order models such as the Lighthill-Whitham-Richards conservation law model. We will have more to say about this in Section 3.4.1.

On the other hand, the one-argument emission functions typically depend on the average speed. Rose et al. (1965) show that when traveling speed is under 80 km/hour, the relation between speed v (in km/hour) and HC/CO emissions e_x (in pound/km) can be approximated by (for now and sequel, e_x denote the emission per unit distance).

$$e_x \;=\; b_1\, v^{-b_2} \tag{1.3}$$

where b_1, b_2 are parameters depending on vehicle type and surrounding environment. Kent and Mudford (1979) collected driving pattern data in Sydney and found that NO_y emission $\tilde{e}_x$ can be modeled by

$$\tilde{e}_x \;=\; \tilde{b}_1 + \frac{\tilde{b}_2}{v} \tag{1.4}$$

According to the Emission Factor Model 2000 CARB (2000) by California Air Resources Board, constantly updated since 1988, the hot running emissions per unit distance

$$\hat{e}_x \;=\; \text{BER} \times \exp\left\{\hat{b}_1(v-17.03) + \hat{b}_2(v-17.03)^2\right\} \tag{1.5}$$

where BER stands for basic emission rates, which are constants associated with CO, NO_y, HC. The unit of velocity is in miles/hour, the unit of $\hat{e}_x$ is in grams/mile.

1.2.4 Solving MPEC problems

The mathematical program with equilibrium constraints (MPEC), by its bi-level and non-convex nature, often creates computational difficulties. A common approach to solve an MPEC problem is to reformulate the bi-level program into a *mathematical program with complementarity constraints* (MPCC). (See Ban et al., 2006; Friesz, 2010). However, as noted by Rodrigues and Monteiro (2006) and Ban et al. (2006), the complementarity constraints might lose certain constraint qualifications. To resolve this issue, some regularization techniques are proposed in the literature. Ralph and Wright (2004) study a relaxation approach, which is then applied by Ban et al. (2006) to solve a continuous network design problem. Anitescu (2000) proposes an l_1-penalty approach and studies its impact on the convergence of an interior point algorithm; while Monteiro and Meira (2011) test a quadratic penalty function. According to their numerical results, quadratic penalty is a promising approach to handle complementarity constraints. However, all of the discussions above focus on MPCC or MPEC in the context of finite dimensional programs. Regarding continuous-time dynamic MPECs, numerical techniques were scarcely visited. Existing literature on continuous-time MPECs includes the single-level reformulation proposed by Friesz et al. (2007), the metaheuristic approach by Yao et al. (2012) and a simultaneous discretization-based method by Raghunathan et al. (2004).

This project utilizes the quadratic penalty method to solve the proposed dynamic MPEC problem. In particular, we will drop the complementarity constraints from the MPCC reformulation, and attach to the objective function a quadratic penalty function for the dropped constraints. The numerical results show general solvability and effectiveness of the proposed numerical method.

2 A robust optimization approach for dynamic traffic signal control with emission constraints

2.1 Formulation of the traffic signal control problem using the variational theory

This section recaps the link-based kinematic wave model (LKWM) proposed by Han et al. (2012) in continuous time, whose discrete time counterpart is equivalent to the link transmission model (LTM) discussed by Yperman et al. (2005). The problem of optimal signal control is then formulated, based on the LKWM, as a mixed-integer linear program in discrete time.

2.1.1 Lighthill-Whitham-Richards model

Following the classical model introduced by Lighthill and Whitham (1955) and Richards (1956), we model the traffic dynamics on a link with the following first order *partial differential equation* (PDE), which describes the spatial-temporal evolution of density and flow

$$\frac{\partial}{\partial t}\rho(t,\,x) + \frac{\partial}{\partial x} f\big(\rho(t,\,x)\big) \;=\; 0 \tag{2.6}$$

where $\rho(t,\, x) : [0,\, +\infty) \times [a,\, b] \to [0,\, \rho_j]$ is average vehicle density, $f(\rho) : [0,\, \rho^{jam}] \to [0,\, C]$ is average flow. ρ^{jam} is jam density, C is flow capacity. The function $f(\cdot)$ articulates a density-flow relation and is commonly referred to as the fundamental diagram.

Classical mathematical results on the first-order hyperbolic equations of the form (2.6) can be found in Bressan (2000). For a detailed discussion of numerical schemes for conservation laws, we refer the reader to Godunov (1959) and LeVeque (1992). A well-known discrete version of the LWR model, the Cell Transmission Model (CTM), was introduced by Daganzo (1994, 1995); the latter reference also extends the discrete dynamic to network structures through straightforward bookkeeping. Other studies of the network extension of the LWR model or the CTM include Bretti et al. (2006), Coclite et al (2005), Herty and Klar (2003), Holden and Risebro (1995), Jin (2010), Jin and Zhang (2003), Lebacque and Khoshyaran (1999), and Lebacque and Khoshyaran (2002).

Let us introduce function $N(\cdot,\, \cdot) : [0,\, +\infty) \times [a,\, b] \to \mathbb{R}$, such that

$$\frac{\partial}{\partial x} N(t,\, x) \;=\; -\,\rho(t,\, x), \qquad \frac{\partial}{\partial t} N(t,\, x) \;=\; f\big(\rho(t,\, x)\big). \tag{2.7}$$

Function $N(t,\, x)$ is sometimes referred to as the Moskowitz function or the Newell-curves. It has been studied extensively, for example, by Claudel and Bayen (2010); Daganzo (2005); Moskowitz (1965); Newell (1993). A well-known property of $N(\cdot,\, \cdot)$ is that it satisfies the following Hamilton-Jacobi equation

$$\frac{\partial}{\partial t} N(t,\, x) - f\left(-\frac{\partial}{\partial x} N(t,\, x)\right) \;=\; 0 \qquad (t,\, x) \in [0,\, +\infty) \times [a,\, b] \tag{2.8}$$

2.1.2 Link dynamics

Let us consider a homogeneous link $[a,\, b]$, whose dynamic is governed by the LWR model. A triangular fundamental diagram is assumed, which takes the following form:

$$f(\rho) \;=\; \begin{cases} k\rho & \rho \in [0,\, \rho^*] \\ -w(\rho - \rho_{jam}) & \rho \in (\rho^*,\, \rho_{jam}] \end{cases} \tag{2.9}$$

where k and w denote, respectively, the forward and backward propagating speeds of kinematic waves; ρ^* denotes the critical density at which the flow is maximized; and ρ_{jam} represents the jam density.

Define a binary variable $\bar{r}(t)$ that indicates whether the entrance of the link is in the free-flow phase ($\bar{r}(t) = 0$) or in the congested phase ($\bar{r}(t) = 1$). A similar notation $\hat{r}(t)$ is used for the exit of the link. We also define the entering flow $\bar{q}(t)$ and the exiting flow $\hat{q}(t)$ of the link. The variational theory in Aubin et al. (2008), Daganzo (2005), and Han et al. (2012) then asserts that

$$\bar{r}(t) = \begin{cases} 1, & \text{if} \quad \int_0^t \bar{q}(\tau)\, d\tau \;=\; \int_0^{t-\frac{L}{w}} \hat{q}(\tau)\, d\tau + \rho_j L \\ 0, & \text{if} \quad \int_0^t \bar{q}(\tau)\, d\tau \;<\; \int_0^{t-\frac{L}{w}} \hat{q}(\tau)\, d\tau + \rho_j L \end{cases} \tag{2.10}$$

$$\hat{r}(t) = \begin{cases} 0, & \text{if} \quad \int_0^{t-\frac{L}{k}} \bar{q}(\tau)\, d\tau \;=\; \int_0^t \hat{q}(\tau)\, d\tau \\ 1, & \text{if} \quad \int_0^{t-\frac{L}{k}} \bar{q}(\tau)\, d\tau \;>\; \int_0^t \hat{q}(\tau)\, d\tau \end{cases} \tag{2.11}$$

where L denotes the link length.

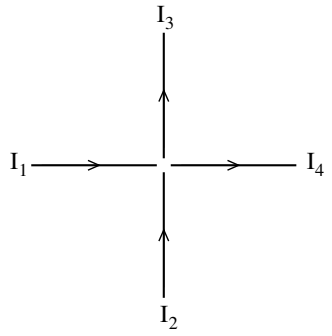

Figure 1: A signalized junction with two incoming links and two outgoing links.

2.1.3 Dynamics at signalized intersections

Without loss of generality, we relate our discussion of the dynamics on signalized networks to the following junction depicted in Figure 1.
Such a junction has two incoming links I_1, I_2, and two outgoing links I_3, I_4. Each link is expressed as a spatial interval $[a_i, b_i]$, $i = 1, 2, 3, 4$. The fundamental diagram of road traffic on each link is given by

$$f_i(\rho) \;=\; \begin{cases} k_i\,\rho & \rho \in [0,\, \rho_i^*] \\ -w_i\,(\rho - \rho_i^{jam}) & \rho \in (\rho_i^*,\, \rho_i^{jam}] \end{cases} \qquad i \;=\; 1,\, 2,\, 3,\, 4$$

with $C_i \doteq k_i\,\rho_i^*$ being the flow capacity. We make the following assumption.
(A) Drivers arriving at the junction distribute on the outgoing roads according to some known coefficients:

$$A \;=\; \begin{pmatrix} \alpha_{1,3} & \alpha_{1,4} \\ \alpha_{2,3} & \alpha_{2,4} \end{pmatrix}$$

where α_{ij} denotes the percentage of traffic coming from link I_i that distributes to outgoing link I_j.

We next introduce the concepts of link demand and link supply, originally articulated by Lebacque and Khoshyaran (1999, 2002). The link demand and supply for I_i, denoted by $D_i(t)$ and $S_i(t)$ respectively, are determined as follows

$$D_i(t) \;=\; \begin{cases} C_i & \text{if } \hat{r}_i(t) \;=\; 1 \\ f_i\big(\rho_i(t,\, b_i-)\big) & \text{if } \hat{r}_i(t) \;=\; 0 \end{cases} \qquad i = 1,\, 2 \tag{2.12}$$

$$S_j(t) \;=\; \begin{cases} C_j & \text{if } \bar{r}_j(t) \;=\; 0 \\ f_j\big(\rho_j(t,\, a_j+)\big) & \text{if } \bar{r}_j(t) \;=\; 1 \end{cases} \qquad j = 3,\, 4 \tag{2.13}$$

Notice that in the case of a triangular fundamental diagram, the profiles of density/flow always translate linearly until they encounter a shock wave. In other words, if $\hat{r}_i(t) = 0$ for some time t, then the whole link remains in the uncongested phase. As a result, we have

$$f_i\big(\rho_i(t,\, b_i-)\big) \;=\; f_i\left(\rho_i\big(t - \frac{L_i}{k_i},\, a_i + \big)\right) \;=\; \bar{q}_i\left(t - \frac{L_i}{k_i}\right) \qquad i = 1,\, 2$$

Similarly we have that

$$f_j\big(\rho_j(t,\, a_j+)\big) \;=\; f_j\left(\rho_j\big(t - \frac{L_j}{w_j},\, b_j + \big)\right) \;=\; \hat{q}_j\left(t - \frac{L_j}{w_j}\right) \qquad j = 3,\, 4$$

so that (2.12) and (2.13) can be re-written as

$$D_i(t) \;=\; \begin{cases} C_i & \text{if } \hat{r}_i(t) \;=\; 1 \\ \bar{q}_i\left(t - \frac{L_i}{k_i}\right) & \text{if } \hat{r}_i(t) \;=\; 0 \end{cases} \qquad i = 1,\, 2 \tag{2.14}$$

$$S_j(t) \;=\; \begin{cases} C_j & \text{if } \bar{r}_j(t) \;=\; 0 \\ \hat{q}_j\left(t - \frac{L_j}{w_j}\right) & \text{if } \bar{r}_j(t) \;=\; 1 \end{cases} \qquad j = 3,\, 4 \tag{2.15}$$

Let us consider piecewise-constant control functions $u_1(t)$ and $u_2(t) \in \{0,\, 1\}$, such that

$$u_1(t) \;=\; \begin{cases} 1 & \text{when the signal is green for } I_1 \\ 0 & \text{when the signal is red for } I_1 \end{cases} \tag{2.16}$$

$$u_2(t) \;=\; \begin{cases} 1 & \text{when the signal is green for } I_2 \\ 0 & \text{when the signal is red for } I_2 \end{cases} \tag{2.17}$$

One obvious identity that must be satisfied by these controls is $u_1(t) + u_2(t) \equiv 1$, for all t. Finally, we can now express the flow propagation across the signalized intersection as

$$\begin{array}{rcl} \hat{q}_1(t) & = & \min\left\{D_1(t),\, \min\{\frac{S_3(t)}{\alpha_{1,3}},\, \frac{S_4(t)}{\alpha_{1,4}}\} \cdot u_1(t)\right\} \\ \hat{q}_2(t) & = & \min\left\{D_2(t),\, \min\{\frac{S_3(t)}{\alpha_{2,3}},\, \frac{S_4(t)}{\alpha_{2,4}}\} \cdot u_2(t)\right\} \\ \bar{q}_3^k & = & \alpha_{1,3}\hat{q}_1(t) + \alpha_{2,3}\hat{q}_2(t), \qquad \bar{q}_4(t) \;=\; \alpha_{1,4}\hat{q}_1(t) + \alpha_{2,4}\hat{q}_2(t) \end{array} \tag{2.18}$$

Remark 2.1. *In principle, the vehicle turning distribution matrix $A = (\alpha_{ij})$ is allowed to be time-dependent. The dynamics conveyed by* (2.18) *remain valid.*

2.1.4 Continuous-time formulation

In this section, we summarize the previous discussion on the flow propagation constraints. Later in the next section, a discrete time version will be presented which serves as the constraints of the proposed mixed-integer linear program.

Let us fix the planning horizon $[0,\, T]$ for some fixed $T > 0$. Introducing the piecewise-constant control variables $u_i(\cdot) : [0,\, T] \to \{0,\, 1\}$, $i = 1,\, 2$, with the agreement that $u_i(t) = 0$ if the light is red for link I_i, and $u_i(t) = 1$ if the light is green for link I_i. It is convenient to use the following set of notations. For $i = 1,\, 2,\, 3,\, 4$.

$\bar{q}_i(\cdot)$,	the flow of cars entering link I_i,
$\hat{q}_i(\cdot)$,	the flow of cars exiting link I_i,
$\bar{r}_i(\cdot)$,	the binary variable that indicates the regime at $x \;=\; a_i+$,
$\hat{r}_i(\cdot)$,	the binary variable that indicates the regime at $x \;=\; b_i-$,
$\bar{q}_i^{max}(\cdot)$,	the maximum flow allowed to enter the link I_i,
$\hat{q}_i^{max}(\cdot)$,	the maximum flow allowed to exit the link I_i,
$N_{up,i}(\cdot)$,	the cumulative number of cars that have entered link I_i,
$N_{down,i}(\cdot)$,	the cumulative number of cars that have exited link I_i,
$u_i(\cdot)$,	the signal control variable for link I_i,

Theorem 2.2. *The dynamics at the signalized intersection visualized in Figure 1 can be described by the following system of differential algebraic equations (DAE) with binary variables.*

$$\frac{d}{dt}N_{up,i}(t) = \bar{q}_i(t), \qquad \frac{d}{dt}N_{down,i}(t) = \hat{q}_i(t), \qquad i = 1,\, 2,\, 3,\, 4 \tag{2.19}$$

$$\bar{r}_i(t) = \begin{cases} 1, & \text{if} \quad N_{up,i}(t) \geq N_{down,i}\left(t - \frac{L_i}{w_i}\right) + \rho_i^{jam} L_i \\ 0, & \text{otherwise} \end{cases}, \quad i = 1,\, 2,\, 3,\, 4 \tag{2.20}$$

$$\hat{r}_i(t) = \begin{cases} 0, & \text{if} \quad N_{up,i}\left(t - \frac{L_i}{k_i}\right) \leq N_{down,i}(t) \\ 1, & \text{otherwise} \end{cases}, \qquad i = 1,\, 2,\, 3,\, 4 \tag{2.21}$$

$$\bar{q}_i^{max}(t) = C_i + \bar{r}_i(t)\left(\hat{q}_i\left(t - \frac{L_i}{w_i}\right) - C_i\right), \qquad i = 1,\, 2 \tag{2.22}$$

$$\hat{q}_i^{max}(t) = \bar{q}_i\left(t - \frac{L_i}{k_i}\right) + \hat{r}_i(t)\left(C_i - \bar{q}_i\left(t - \frac{L_i}{k_i}\right)\right), \qquad i = 3,\, 4 \tag{2.23}$$

$$\hat{q}_i(t) = \begin{cases} 0, & \text{if} \quad u_i(t) = 0 \\ \min\left\{\hat{q}_i^{max}(t),\, \frac{\bar{q}_3^{max}(t)}{\alpha_{i,3}},\, \frac{\bar{q}_4^{max}(t)}{\alpha_{i,4}}\right\} & \text{if} \quad u_i(t) = 1 \end{cases}, \quad i = 1,\, 2 \tag{2.24}$$

$$\bar{q}_k(t) = \alpha_{1,k}\,\hat{q}_1(t) + \alpha_{2,k}\,\hat{q}_2(t), \qquad k = 3,\, 4, \tag{2.25}$$

$$u_1(t) + u_2(t) = 1 \qquad \text{for all} \;\; t \in [0,\, T] \tag{2.26}$$

Proof. The proof is straightforward. □

2.1.5 Discrete-time formulation

In this section, we present the discrete-time version of the optimization problem in Theorem 2.2. Let us introduce a few more notations for the convenience of our presentation. Consider a uniform time grid

$$0 \;=\; t^0 \;<\; t^1 \;\ldots\; <\; t^N \;=\; T, \qquad t^j - t^{j-1} \;=\; \delta t, \quad j \;=\; 1, \ldots, N$$

Throughout the rest of this report, we use superscript 'j' to denote the discrete value evaluated at time step t^j. In addition, we let $L_i/k_i = \Delta_i^f \delta t$, $L_i/w_i = \Delta_i^b \delta t$, $\Delta_i^f \in \mathbb{N}$, $\Delta_i^b \in \mathbb{N}$, $i = 1, 2, 3, 4$.

Approximating the numerical integration with rectangular quadratures, we write equality (2.20) and (2.21) in discrete time as

$$\begin{cases} \delta t \sum_{j=0}^{k-\Delta_i^b} \hat{q}_i^j - \delta t \sum_{j=0}^{k} \bar{q}_i^j + \rho^{jam} L_i \;\leq\; \mathcal{M}\,(1 - \bar{r}_i^k) \\ \delta t \sum_{j=0}^{k-\Delta_i^b} \hat{q}_i^j - \delta t \sum_{j=0}^{k} \bar{q}_i^j + \rho^{jam} L_i \;\geq\; -\mathcal{M}\,\bar{r}_i^k + \varepsilon \end{cases} \qquad \Delta_i^b \;\leq\; k \;\leq\; N, \quad i \;=\; 1,\, 2,\, 3,\, 4 \tag{2.27}$$

$$\begin{cases} \delta t \sum_{j=0}^{k-\Delta_i^f} \bar{q}_i^j - \delta t \sum_{j=0}^{k} \hat{q}_i^j \;\leq\; \mathcal{M}\,\hat{r}_i^k \\ \delta t \sum_{j=0}^{k-\Delta_i^f} \bar{q}_i^j - \delta t \sum_{j=0}^{k} \hat{q}_i^j \;\geq\; \mathcal{M}\,(\hat{r}_i^k - 1) + \varepsilon \end{cases} \qquad \Delta_i^f \;\leq\; k \;\leq\; N, \quad i \;=\; 1,\, 2,\, 3,\, 4 \tag{2.28}$$

where $\bar{r}_i^k$, $\hat{r}_i^k \in \{0, 1\}$. $\mathcal{M} \in \mathbb{R}_+$ is a sufficiently large number, $\varepsilon \in \mathbb{R}_+$ is a sufficiently small number. Constraints (2.27) and (2.28) determine the regime variables associated with the two boundaries of each link. Once the flow phases are determined, the demand and supply functions (2.22), (2.23) are rewritten in discrete time as

$$\begin{cases} C_i - \mathcal{M}\,\bar{r}_i^j \;\le\; \bar{q}_i^{max,j} \;\le\; C_i \\ \hat{q}_i^{j-\Delta_i^b} - \mathcal{M}\,(1-\bar{r}_i^j) \;\le\; \bar{q}_i^{max,j} \;\le\; \hat{q}_i^{j-\Delta_i^b} + \mathcal{M}\,(1-\bar{r}_i^j) \end{cases} \qquad i \;=\; 1,\, 2,\, 3,\, 4 \tag{2.29}$$

$$\begin{cases} C_i + \mathcal{M}\,(\hat{r}_i^j - 1) \;\le\; \hat{q}_i^{max,j} \;\le\; C_i \\ \bar{q}_i^{j-\Delta_i^f} - \mathcal{M}\,\hat{r}_i^j \;\le\; \hat{q}_i^{max,j} \;\le\; \bar{q}_i^{j-\Delta_i^f} + \mathcal{M}\,\hat{r}_i^j \end{cases} \qquad i \;=\; 1,\, 2,\, 3,\, 4 \tag{2.30}$$

Next, let us reformulate (2.24). Introducing dummy variables ζ_1^j, ζ_2^j, $1 \le j \le N$, such that

$$\zeta_i^j \;=\; \min\left\{ \hat{q}_i^{max,j},\, \frac{\bar{q}_3^{max,j}}{\alpha_{i,3}}\, \frac{\bar{q}_4^{max,j}}{\alpha_{i,4}} \right\} \qquad i \;=\; 1,\, 2 \tag{2.31}$$

Then the discrete-time version of (2.24) can be readily written as

$$\begin{cases} 0 \;\le\; \hat{q}_i^j \;\le\; \mathcal{M}\,u_i^j \\ \zeta_1^j + \mathcal{M}\,(u_i^j - 1) \;\le\; \hat{q}_i^j \;\le\; \zeta_1^j \end{cases} \qquad i \;=\; 1,\, 2, \quad j \;=\; 1, \ldots, N \tag{2.32}$$

In order to write (2.31) as linear constraints, one could write it as three "less or equal" statements, which is simple but bears the potential limitation of traffic holding. Instead, one may introduce additional binary variables ξ_i^j, η_i^j and real variables β_i^j for $i = 1,\, 2$, $j = 1, \ldots, N$, such that (2.31) can be accurately formulated as

$$\begin{cases} \bar{q}_3^{max,j}/\alpha_{i,3} - \mathcal{M}\,\xi_i^j \;\le\; \beta_i^j \;\le\; \bar{q}_3^{max,j}/\alpha_{i,3} \\ \bar{q}_4^{max,j}/\alpha_{i,4} - \mathcal{M}\,(1-\xi_i^j) \;\le\; \beta_i^j \;\le\; \bar{q}_4^{max,j}/\alpha_{i,4} \\ \hat{q}_i^{max,j} - \mathcal{M}\,\eta_i^j \;\le\; \zeta_i^j \;\le\; \hat{q}_i^{max,j} \\ \beta_i^j - \mathcal{M}\,(1-\eta_i^j) \;\le\; \zeta_i^j \;\le\; \beta_i^j \end{cases} \qquad i \;=\; 1,\, 2 \tag{2.33}$$

Finally, we have the obvious relations

$$\bar{q}_k^j(t) \;=\; \alpha_{1,k}\hat{q}_1^j(t) + \alpha_{2,k}\hat{q}_2^j(t) \qquad k \;=\; 3,\, 4, \qquad j \;=\; 1, \ldots, N \tag{2.34}$$

and

$$u_1^j + u_2^j \;=\; 1 \qquad j \;=\; 1, \ldots, N \tag{2.35}$$

The proposed MILP formulation of signal control problem is summarized by (2.27)-(2.30) and (2.32)-(2.35). This formulation captures many desirable features of vehicular flow on networks such as physical queues, spill back, vehicle turning, and shock formation and propagation (although not explicitly). The signal control allows time-varying cycle length and splits, as well as the utilization of real-time information of traffic flows.

2.2 Macroscopic relationship between the emission rate and traffic quantities

As mentioned in the introductory part of this report, the application of robust optimization techniques to handle emission constraints requires a well-defined and calibrated macroscopic relationship between the emission rate at a link level and certain macroscopic traffic quantities. In this section,

we will explore such potential relationships through numerical simulation that employs the link-based kinematic wave model (link transmission model) as means of propagating flow through links and junctions, as well as two different emission models: the average-speed emission model and the modal emission model.

We consider a homogeneous link I_i in which traffic states are described by a triangular fundamental diagram. To obtain the desired correlations between emissions and macroscopic traffic parameters, we simulate various scenarios of free-flow, capacity, and congested conditions on the link. To this end, we randomly generate demand and supply profiles at places immediately upstream and downstream to the link under consideration[1]. In addition, since we are mainly interested in estimating emission in traffic stream controlled by signals, the generation of demand and supply profiles is consistent with scenarios where signal controls are present. More specifically, we randomly generate binary variables corresponding to signal controls at both places upstream and downstream to the link of interest. Such choice of link boundary flows will generate stop-and-go waves and vehicle stops, which are considered a major source of the most harmful emissions near signalized intersections.

Once the boundary conditions are given for each simulation run, we solve the Hamilton-Jacobi equation in discrete space-time using a variational approach known as the Lax-Hopf formula in Aubin et al. (2008), Claudel and Bayen (2010), and Han et al. (2012). Solution of the H-J equation provides critical information on vehicle densities, speeds, and acceleration, which are then used, in combination with a specific emissions model, to calculate the total emission rate at a link level.

In the next two subsections, Section 2.2.1 and Section 2.2.2, we will use two different emission models to numerically validate the hypothesized macroscopic relationship between aggregated emission rate and link occupancy. Details on the simulations runs as well as methods for computing emissions will be presented. Without loss of generality, all numerical simulations are performed for a single link with a triangular fundamental diagram with the following parameters:

$k = 13.33$ meter/second, $w = 4.44$ meter/second, $\rho^{jam} = 0.4$ vehicle/meter, $C = 1.33$ vehicle/second

where k denotes the free-flow speed, w is the speed of backward-propagating kinematic waves, ρ^{jam} denotes the jam density, and C is the flow capacity.

2.2.1 The average-speed emission model

As our first emission model, we consider a relatively simple speed-based emission model expressed as follows.

$$e_t \;=\; \Upsilon(v) \tag{2.36}$$

where v (in mile/hour) is the (average) velocity of the vehicle and e_t (in gram/hour) is the corresponding emission rate. The aggregate emission rate (AER) on link I_l at time t is calculated as:

$$\mathrm{AER}_l(t) \;=\; \int_{a_l}^{b_l} \rho_l(t,\,x)\Upsilon\left(v_l\big(\rho_l(t,\,x)\big)\right)\,dx \qquad t \in [0,\,T] \tag{2.37}$$

where the link I_l is expressed as a spatial interval $[a_l,\,b_l]$; $\rho_l(t,\,x)$ is the solution of the LWR PDE (2.6) and represents vehicle density; and the velocity $v_l = v_l\big(\rho_l(t,\,x)\big)$ is a function of density defined via the fundamental diagram $f_l(\cdot)$. The link occupancy $N_l(t)$ at each instance of time is easily computed as

$$N_l(t) \;=\; \int_{a_l}^{b_l} \rho_l(t,\,x)\,dx \qquad t \in [0,\,T] \tag{2.38}$$

[1]The terminologies 'demand' and 'supply' coincide with those articulated by Lebacque and Khoshyaran (1999, 2002). In terms of solving the Hamilton-Jacobi equation equivalent to (2.6), the demand and supply curves correspond to the notion of weak boundary conditions illustrated in Aubin et al. (2008).

Another way of expressing the link occupancy is through the cumulative boundary curves as follows

$$N_l(t) \;=\; \int_0^t f_l\left(\rho_l(s,\, a_l)\right)\, ds - \int_0^t f_l\left(\rho_l(s,\, b_l)\right)\, ds \tag{2.39}$$

For the functional form of $\Upsilon(v)$, we employ the speed-based model TRANSYT-7F for CO emissions that has been used by several other studies in the literature by Benedek and Rilett (1998), Penic and Upchurch (1992), and Nagurney et al. (2010), noting that other types of speed-based emission models can be equally applied.

$$e_x \;=\; 26.3009 \cdot \frac{\exp(0.009928\, v)}{v} \tag{2.40}$$

where v is in miles/hour and e_x (in grams/mile) is the amount of CO emissions per unit travel distance. Note that the notation e_x is meant to indicate that the emission rate is in terms of amount per unit distance. This quantity can be easily converted to represent amount per unit time (in grams/hour) by using the following trick.

$$e_t \;=\; \frac{\partial e}{\partial t} \;=\; \frac{\partial e}{\partial x} \cdot \frac{\partial x}{\partial t} \;=\; e_x \cdot v \;=\; 26.3009 \cdot \exp(0.009928\, v) \tag{2.41}$$

Identity (2.41) is used to determine the emission rate when traffic density is relatively stable, for example, in a cell where density is uniformly distributed. The average emissions rate for the link is then computed from (2.37).

Details of the simulation are as follows. We first randomly generate the demand and supply functions for the upstream and downstream boundaries of the link, respectively. The values of demand and supply are uniformly distributed between zero and the link flow capacity to account for different levels of congestion. Moreover, in order to be consistent with signal controls present at both ends of the link, we generate "red" and "green" periods to control cars that enter or exit the link of interest. The lengths of those "red" or "green" periods are uniformly distributed within [10, 40] (in seconds).

In a single simulation run, given a boundary condition, we solve the LWR PDE (2.6) by first applying the variational method to the Hamilton-Jacobi equation (2.8) and then by differentiating the Moskowitz function. Alternatively, one may solve the scalar conservation law directly using the Godunov scheme in Godunov (1959) or the cell transmission model in Daganzo (1994). Once vehicle densities are available in discrete space and time, we then use the fundamental diagram to find the corresponding vehicle speeds and come up with emission estimation according to (2.41) and (2.37).

The simulation result is shown in Figure 2, which contains 40,000 samples. There clearly exists a macroscopic relationship between the link occupancy (LO) and the link aggregate emission rate (AER). In addition, a simple regression shows that such relationship is affine, as shown below with $R^2 = 0.9990$:

$$AER \;=\; 26.13 \times LO + 89.94$$

where AER is in gram/hour, and LO is in vehicle.

The well-defined affine relationship can be explained by the fact that the emission model only takes into account the velocity, which varies between 0 and the free-flow speed 13.3 (meter/second). Thus the emission rate of a single vehicle, according to formula (2.41), varies within [26.3, 30.0] (gram/hour). With such a relatively small variation in the emission rate, the aggregate emission rate on a link level is almost proportional to the number of vehicles present regardless of the spatial distribution or the operational modes of those vehicles, which is predicted by the LWR model.

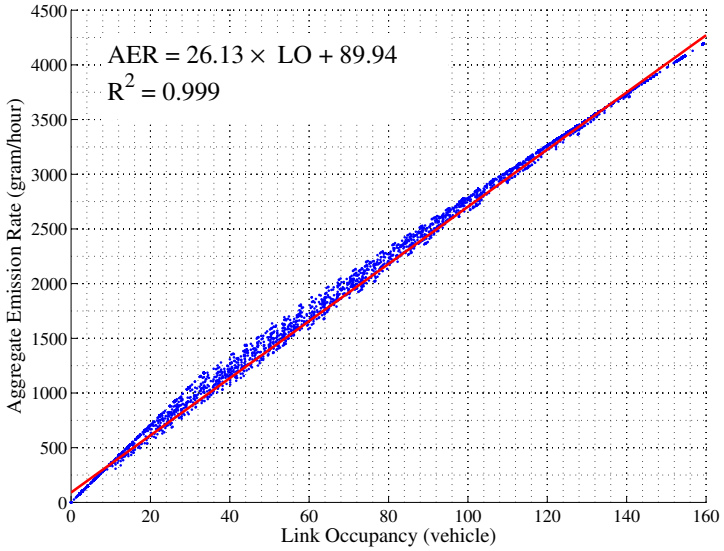

Figure 2: The speed-based emission model: Scatter plot of link occupancy verses AER.

2.2.2 The modal emission model

The second emissions model that we consider directly accounts for the modal operation of a vehicle; that is, the emissions are directly related to vehicle operating modes such as idle, steady-state cruise, acceleration, and deceleration. This model relies on trajectories of moving vehicles, which can be estimated from the LWR model. More specifically, let $\rho_l(t,\, x)$ be the solution of the scalar conservation law (2.6) on link I_l; the local velocity $v_l(t,\, x)$ of vehicles is computed as $v_l(t,\, x) = f_l(\rho_l(t,\, x))/\rho_l(t,\, x)$. The acceleration/deceleration, $a_l(t,\, x)$, viewed as the derivative of the velocity along the trajectory of a single vehicle, is computed as the material derivative in the Eulerian coordinates:

$$a_l(t,\, x) \;=\; \frac{D}{Dt} v_l(t,\, x) \;=\; \partial_t v_l(t,\, x) + v_l(t,\, x) \cdot \partial_x v_l(t,\, x)$$

Since the quantities $\rho_l(t,\, x)$ and $v_l(t,\, x)$ are in general non-differentiable, they are approximated in discrete time as finite differences. Let $\{t_i\}$ and $\{x_j\}$ be discrete temporal and spatial grid points, then we have

$$a_l(t_i,\, x_j) \;=\; \frac{v_l(t_{i+1},\, x_j) - v_l(t_{i-1},\, x_j)}{2\delta t} + v_l(t_i,\, x_j) \cdot \frac{v_l(t_i,\, x_{j+1}) - v_l(t_i,\, x_{j-1})}{2\delta x} \tag{2.42}$$

where δt and δx are constant time step and spatial step, respectively. According to the power demand-based emission model proposed by Post et al. (1984), the overall instantaneous total power demand Z (in kilowatts) for a vehicle with mass m (in kilograms) is given by

$$Z \;=\; (0.04\, v + 0.5 \times 10^{-3} v^2 + 10.8 \times 10^{-6} v^3) + \frac{m}{1000} \frac{v}{3.6} \left(\frac{a}{3.6} + 9.81 \sin\theta \right) \tag{2.43}$$

where the above quantity is in kilowatts and θ denotes the roadway grade. The reader is also referred to Barth et al. (1996) for an alternative description of the power demand function based on velocity and acceleration. Post et al. (1984) also propose the following model of hydrocarbon emissions rate for spark ignition vehicles:

$$r(t) \;=\; \begin{cases} 52.8 + 4.2Z & Z \;>\; 0 \\ 52.8 & Z \;\leq\; 0 \end{cases} \tag{2.44}$$

based on field experiments, where the emission rate $r(t)$ is in grams/hour, and Z is in kilowatts.

Following the preceding discussion, we now compute the aggregate emission rate (AER) in discrete time as

$$AER_l(t_i) \;=\; \sum_j \rho_l(t_i,\, x_j) r_l(t_i,\, x_j)$$

where $r_l(t_i,\, x_j)$ is the emission rate inside the j-th cell and is calculated using (2.42), (2.43), and (2.44).

Our simulation results are shown in Figure 3, which contains 40,000 samples. Notice that although with a larger variation than the previous case, we still observe a reasonable affine relationship between the link occupancy and the AER. The best linear fit is given by

$$AER \;=\; 52.31 \times LO + 318.63$$

with $R^2 = 0.9794$.

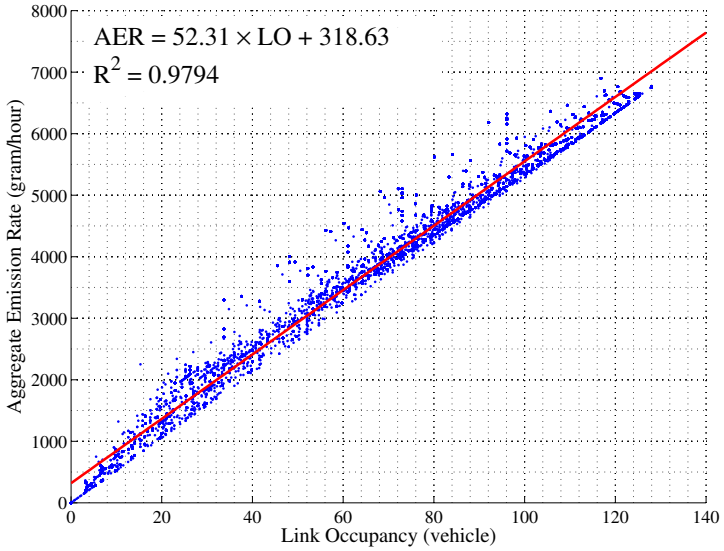

Figure 3: Scatter plot of link occupancy verses AER.

The larger variations in the AER are expected, as it is due to the highly nonlinear effect caused by vehicle acceleration and deceleration. In a typical signalized intersection modeled by the LWR equation, the shock waves generated by signal timing cause stop-and-go patterns which greatly increases vehicle acceleration/deceleration and hence emission amount. Moreover, these patterns are dependent on the actual spatial configuration of the vehicle densities, which cannot be adequately captured by the link occupancy.

A macroscopic relationship depicted in Figure 3 is more interesting from a robust optimization perspective than that in Figure 2. The reason is that although all points are distributed within a tube-shape region (see Figure 3), they are sparse in some places while dense in some others. An uncertainty region that simply covers all these points may be too conservative, and a more effective approach calls for a careful calibration of the uncertainty set. This will be presented in our numerical study in Section 2.5.

2.3 Emission-related side constraints

In this section, we propose a set of emission-related constraints constructed in a data-driven manner that employ robust optimization techniques to handle parameter errors arising from the macroscopic relationship between emission rates and link occupancy, as we observed in the previous section. In addition, we show that when this relationship can be captured by an affine or a convex/concave piecewise affine function, the resulting set of emission-related constraints can maintain linearity. Using notations established in Section 2.1.4, we let $N_i(t) = N_{i,up}(t) - N_{i,down}(t)$ be the total number of vehicles on link $I_i \in \mathbb{I}$ at time t; in other words, it denotes the link occupancy in units of vehicles. The time-varying total emission rates on link I_i is denoted by $\epsilon_i(t)$. Although our previous numerical simulations suggest an approximately affine relationship between $N_i(t)$ and $\epsilon_i(t)$, in the following derivation of emission constraints we assume a more general functional form for such relationship, so that the proposed methodology will apply to a class of more general macroscopic relationships.

We assume that such a relationship is approximated by a polynomial with power $\mathcal{L}$, where the approximation is based on regression analysis or other types of curve-fitting techniques:

$$\epsilon_i(\boldsymbol{a},\ N_i(t)) \ = \ \sum_{l=0}^{\mathcal{L}} a_l (N_i(t))^l \ = \ \boldsymbol{a}^T \boldsymbol{N}_i(t) \qquad \text{for all } I_i \in \mathbb{I},\ \text{for all } t \in [0,\, T]. \tag{2.45}$$

Here $\boldsymbol{a} \doteq (a_0,\, a_1,\, \ldots,\, a_{\mathcal{L}})^T$ is the vector of coefficients in the polynomial, and $\boldsymbol{N}_i(t) \doteq \big((N_i(t))^0,\, \ldots,\, (N_i(t))^{\mathcal{L}}\big)$. With these notations, in order to ensure that the total emission amount at each link at any time is constrained by an arbitrarily prescribed level, we have the emission side constraint for link I_i expressed as

$$\int_0^T \epsilon_i(\boldsymbol{a},\ N_i(t))dt \ \leq \ E_i \qquad \text{for all } I_i \in \mathbb{I},\ \text{for all } t \in [0,\, T] \tag{2.46}$$

Such a constraint requires that the emission amount is below some critical value E_i for any link I_i. Notice that such constraints can be easily transformed to address other types of environmental considerations, including:

- the total emissions on the entire network is bounded by some given value, and
- the differences among total emissions of all links are bounded.

The second case ensures that no link (or the neighborhood near that link) suffers much more than other links in terms of air quality. Such an issue is identified by Benedek and Rilett (1998) as *environmental equity*.

In addition, the formulation is also easily extendable to the case where the emission criteria are disutilities to be minimized. In such a case, we may invoke the "epigraph reformulation".

2.3.1 Side constraints considering errors

In (2.46), approximation is involved in the relationship between the vehicle number and the emission amount. In order to ensure that the emission constraint is satisfied even with parameter errors, the following robust constraint is of our interest, instead:

$$\int_0^T \epsilon_i(\boldsymbol{a}(t),\ N_i(t))dt \ \leq \ E_i \qquad \text{for all } \boldsymbol{a}(t) \in \boldsymbol{\eta}_a \tag{2.47}$$

Such a constraint corresponds to the notion of robust optimization in the sense that the emission amount on link I_i is restricted to an upper bound with any possible realization of the parameter $\boldsymbol{a}(t)$. Here by allowing the coefficient $\boldsymbol{a}(t) = (a_l(t) : 0 \leq l \leq \mathcal{L})$ to be varied over time, we have

$$\epsilon_i(\boldsymbol{a}(t),\ N_i(t)) = \sum_{l=0}^{\mathcal{L}} a_l(t)(N_i(t))^l \tag{2.48}$$

and $\boldsymbol{\eta}_a$ is specified as a budget-like uncertainty set, which is similar to that proposed by Atamtürk and Zhang (2007):

$$\boldsymbol{\eta}_a \ = \ \left\{ \boldsymbol{a} :\ L_l \leq a_l(t) \leq U_l,\ \text{for all } 0 \leq l \leq \mathcal{L},\ \sum_{l=1}^{\mathcal{L}} \int_0^T a_l(t)\, dt \ \leq \ \frac{T \sum_{l=1}^{\mathcal{L}} U_l}{\sigma} \right\} \tag{2.49}$$

where L_l and U_l, $0 \leq l \leq \mathcal{L}$, are lower and upper bounds of the coefficients and

$$\sigma \in \left[1,\ \sum_{l=0}^{\mathcal{L}} U_l / \sum_{l=0}^{\mathcal{L}} L_l \right] \tag{2.50}$$

In (2.50), the upper bound on σ ensures that the uncertainty set expressed in (2.49) is nonempty. This can be easily seen by manipulating the last inequality of (2.49):

$$\sum_{l=1}^{\mathcal{L}} T \cdot L_l \ \leq \ \sum_{l=1}^{\mathcal{L}} \int_0^T a_l(t)\, dt \ \leq \ \frac{T \sum_{l=1}^{\mathcal{L}} U_l}{\sigma}$$

Thus σ must not exceed $\sum_{l=0}^{\mathcal{L}} U_l / \sum_{l=0}^{\mathcal{L}} L_l$.

The uncertainty set in (2.49) consists of two types of constraints: (1) a box constraint prescribing the upper bound and the lower bound of the uncertain parameters, and (2) a constraint that prescribes the sums of uncertain coefficients in the l-th order terms $1 \leq l \leq \mathcal{L}$ to be bounded from above (the last constraint in (2.49)). With just the first type of constraints, the RO will generate the most conservative solution by predicting that all the uncertain parameters are realized at the extreme case against the decision maker. However, such a worst case occurs only with a very low probability in a realistic system, and this conservative solution is most likely to compromise the performance of the resulting system. Use of the second type of constraint can reduce the conservatism by excluding some of the extreme and rare cases.

The second type of constraint is made flexible by adjusting the value of σ. Specifically, a higher value of σ means a smaller uncertainty set, which results in solutions that are more risk-prone (less conservative). In the most conservative case, i.e., $\sigma = 1$, the last constraint in (2.49) is out of effect. Bandi and Bertismas (2012) and Bertsimas et al. (2014) provide data-driven approaches based on probability theory and statistical tests to determine the parameterization of the uncertainty sets in accordance with the observed data. Those approaches provide guarantees for the satisfaction of constraints in a probabilistic sense. We would like to further remark that the second type of constraint may also capture potential correlations among $a_l(t)$, $0 \leq l \leq \mathcal{L}$. However, due to space limitation this aspect of research will not be elaborated upon in this report.

By writing (2.49) we have implicitly assumed that coefficients associated with the zeroth-order term are not correlated with the other coefficients (the summation starts from $l = 1$ instead of $l = 0$). Even though this implicit assumption will result in a more risk-averse formulation, it has a smaller number of constraints and thus lower computational overhead. Details of the reformulation without this assumption will not be provided, but the consequent generalization is a trivial extension.

2.3.2 Discretization and explicit reformulation

Constraint (2.47) can be time-discretized into the following form, where δt denotes the time step.

$$\sum_{k=1}^{N}\sum_{l=0}^{\mathcal{L}} a_{l,k}(N_{i,k})^l \delta t \;\le\; E_i \qquad \text{for all } \hat{\boldsymbol{a}} \in \hat{\boldsymbol{\eta}}_a \tag{2.51}$$

where $a_{l,k}$ corresponds to $a_l(\cdot)$ at the k-th time interval, and $\hat{\boldsymbol{a}} := (a_{l,k} :\; 0 \le l \le \mathcal{L},\; 1 \le k \le N)$. The discrete-time version of the uncertainty set is

$$\hat{\boldsymbol{\eta}}_a = \left\{ \hat{\boldsymbol{a}} : L_l \le a_{l,k} \le U_l, \text{ for all } 0 \le l \le \mathcal{L},\; 1 \le k \le N,\; \sum_{k=1}^{N}\sum_{l=1}^{\mathcal{L}} a_{l,k}\delta t \le \frac{T\sum_{l=1}^{\mathcal{L}} U_l}{\sigma} \right\} \tag{2.52}$$

The constraint (2.51) is in fact a semi-infinite constraint with an infinite index set, which is not directly computable. The following theorem gives its computable reformulation.

Theorem 2.3. *Let $-\infty < L_l < U_l < \infty$ for all $0 \le l \le \mathcal{L}$. If $\hat{\boldsymbol{\eta}}_a$ has nonempty interior, the semi-infinite constraint (2.51) is equivalent to the following set of constraints:*

$$\sum_{l=1}^{\mathcal{L}}\sum_{k=1}^{N} \beta_{l,k}U_l - \sum_{l=1}^{\mathcal{L}}\sum_{k=1}^{N} \gamma_{l,k}L_l + \frac{T\sum_{l=1}^{\mathcal{L}} U_l}{\sigma\delta t}\,\theta + \sum_{k=1}^{N} U_0\,\delta t \;\le\; E_i \tag{2.53}$$

$$s.t.\;\; \beta_{l,k} - \gamma_{l,k} + \theta = (N_{i,k})^l \delta t \qquad \textit{for all}\;\; 1 \le l \le \mathcal{L}, \qquad 1 \le k \le N \tag{2.54}$$

$$\beta_{l,k},\; \gamma_{l,k},\; \theta \ge 0 \qquad \textit{for all}\;\; 1 \le l \le \mathcal{L}, \qquad 1 \le k \le N \tag{2.55}$$

where $\beta_{l,k},\; \gamma_{l,k}$ and θ are dummy variables.

Proof. Constraint (2.51) can be trivially rewritten as:

$$\max_{\hat{\boldsymbol{a}}\in\hat{\boldsymbol{\eta}}_a} \sum_{k=1}^{N}\sum_{l=1}^{\mathcal{L}} a_{l,k}(N_{i,k})^l \delta t + \max_{\hat{\boldsymbol{a}}\in\hat{\boldsymbol{\eta}}_a} \sum_{k=1}^{N} a_{0,k}(N_{i,k})^0 \delta t \le E_i, \tag{2.56}$$

which is equivalent to

$$\max_{\hat{\boldsymbol{a}}\in\hat{\boldsymbol{\eta}}_a} \sum_{k=1}^{N}\sum_{l=1}^{\mathcal{L}} a_{l,k}(N_{i,k})^l \delta t \le E_i - \sum_{k=1}^{N} U_0 \delta t. \tag{2.57}$$

The evaluation of the constraint function involves solving a parametric problem of the form:

$$\max_{\hat{\boldsymbol{a}}} \sum_{k=1}^{N}\sum_{l=1}^{\mathcal{L}} a_{l,k}(N_{i,k})^l \delta t \tag{2.58}$$

$$s.t.\;\; a_{l,k} \le U_l, \text{ for all } 0 \le l \le \mathcal{L},\; 1 \le k \le N \tag{2.59}$$

$$a_{l,k} \ge L_l, \text{ for all } 0 \le l \le \mathcal{L},\; 1 \le k \le N \tag{2.60}$$

$$\sum_{k=1}^{N}\sum_{l=1}^{\mathcal{L}} a_{l,k}\delta t \le \frac{T\sum_{l=1}^{\mathcal{L}} U_l}{\sigma} \tag{2.61}$$

where we treat the $N_{i,k}$ as a constant parameter. Program (2.58)-(2.61) has a dual problem of the following:

$$\min_{\boldsymbol{D}} \sum_{l=1}^{\mathcal{L}} \sum_{k=1}^{N} \beta_{l,k} U_l - \sum_{l=1}^{\mathcal{L}} \sum_{k=1}^{N} \gamma_{l,k} L_l + \frac{T \sum_{l=1}^{\mathcal{L}} U_l}{\sigma \delta t} \theta \tag{2.62}$$

$$s.t. \;\; \beta_{l,k} - \gamma_{l,k} + \theta = (N_{i,k})^l \delta t \qquad \text{for all} \;\; 1 \le l \le \mathcal{L}, \qquad 1 \le k \le N \tag{2.63}$$

$$\beta_{l,k},\; \gamma_{l,k},\; \theta \ge 0 \qquad \text{for all} \;\; 1 \le l \le \mathcal{L}, \qquad 1 \le k \le N \tag{2.64}$$

where $\beta_{l,k}$, $\gamma_{l,k}$ and θ are dual variables corresponding to constraints (2.59), (2.60), and (2.61) Under the assumption that $\hat{\boldsymbol{\eta}}_a$ has nonempty interior, by noticing the compactness of $\hat{\boldsymbol{\eta}}_a$, the primal program (2.58)-(2.61) and the dual program (2.62)-(2.64) have finite solutions and zero duality gap. Moreover, by duality, the objective value of any feasible solution to the dual problem (2.62)-(2.64) provides upper bounds to the primal problem (2.58)-(2.61). Therefore, if there exist $\beta_{l,k}$, $\gamma_{l,k}$ and θ such that (2.63)-(2.64) are satisfied, then if $N_{i,k}$ satisfy (2.53), then (2.57) is satisfied.

On the other hand, if there exists $N_{i,k}$ that satisfy (2.57), then the objective value of the optimal solution to the parametric problem (2.58)-(2.61) is bounded above and thus there exists $\beta_{l,k}$, $\gamma_{l,k}$ and θ such that (2.63)-(2.64) are satisfied. Thus, the equivalence of interest is proved. □

Remark 2.4. *The above theorem is based on the discussions in Ben-Tal and Nemirovski (1999) and Bertsimas et al. (2011a). With this reformulation, the original semi-infinite constraint is now computable with standard nonlinear programming techniques. We refer to the reformulated program with constraints (2.53)-(2.55) as the robust counterpart to the original robust problem.*

2.3.3 A special case when the relationship is affine

In a simple case where the relationship between the vehicle number and the emission rate is approximately affine, the robust reformulation discussed previously can be considerably simplified. Indeed, we can reduce (2.47) to

$$\int_0^T [a_1(t)\,(N_i(t)) + a_0(t)]dt$$

$$= \int_0^T [a_1(t)\,(N_{up,i}(t) - N_{down,i}(t)) + a_0(t)]dt \le E_i, \quad \text{for all } (a_0(t), a_1(t)) \in \boldsymbol{\eta}_a \tag{2.65}$$

where

$$\boldsymbol{\eta}_a = \left\{ (a_0(t),\, a_1(t)) :\;\; L_l \le a_l(t) \le U_l,\; l = 0,\, 1,\;\; \int_0^T a_1(t)dt \le \frac{TU_1}{\sigma} = \frac{N\delta t U_1}{\sigma} \right\} \tag{2.66}$$

With time-discretization, we have the following formulation,

$$\sum_{k=1}^{N} \left[a_{1,k} \left(\delta t \sum_{j=0}^{k} \bar{q}_i^j - \delta t \sum_{j=0}^{k} \hat{q}_i^j \right) + a_{0,k} \right] \delta t \;\; \le \;\; E_i \qquad \text{for all } (a_0,\; a_1) \in \hat{\boldsymbol{\eta}}_a \tag{2.67}$$

where $a_0 := (a_{0,k} : 1 \le k \le N)$, $a_1 := (a_{1,k} : 1 \le k \le N)$. The uncertainty set is given as

$$\hat{\boldsymbol{\eta}}_a = \left\{ (a_0,\, a_1) : L_0 \le a_{0,k} \le U_0,\; L_1 \le a_{1,k} \le U_1, \text{ for all } 1 \le k \le N,\; \sum_{k=1}^{N} a_{1,k} \le \frac{NU_1}{\sigma} \right\} \tag{2.68}$$

With the above uncertainty set, we have the following reformulation treated as a special case of Theorem 2.3.

Corollary 2.5. *If $\hat{\boldsymbol{\eta}}_a$ has nonempty interior, then the semi-infinite constraint* (2.68) *is equivalent to the following set of constraints.*

$$\sum_{k=1}^{N} U_1\beta_k - \sum_{k=1}^{N} L_1\gamma_k + \frac{(N+1)U_1}{\sigma}\theta + (N+1)U_0\,\delta t \;\le\; E_i \tag{2.69}$$

$$\theta + \beta_k - \gamma_k \;=\; \delta t^2 \sum_{j=0}^{k} \bar{q}_i^j - \delta t^2 \sum_{j=0}^{k} \hat{q}_i^j \qquad \textit{for all } k = 0, 1, ..., N \tag{2.70}$$

$$\beta_k,\ \gamma_k,\ \theta \;\ge\; 0 \qquad \textit{for all } k = 0, 1, ..., N \tag{2.71}$$

where β_k, γ_k, θ are dual variables.

Once semi-infinite constraint (2.68) is reformulated as a finite set of linear constraints according to the lemma above, the LWR-E problem with an affine macroscopic relationship can be formulated and solved as a mixed-integer linear program.

2.3.4 Piecewise affine case relationship

To allow for additional flexibility in formulation while preserving the linearity in constraints, it is of particular interest to consider the case when the aggregated relationship between emission rate and the vehicle number is approximated by a piecewise affine function. In this subsection, we will provide formulations that consider this piecewise affine relationship under either of two conditions: (1) the relationship is convex piecewise affine, or (2) the relationship is concave piecewise affine.

Convex piecewise affine

We will show in the following that the previously presented reformulation can be easily extended to the convex piecewise affine case. With some abuse of notations, we denote the function of emission rate at each link I_i at time t as:

$$\epsilon_i(\boldsymbol{b}(t),\ N_i(t)) := \max_{m\in\mathbb{M}}(b_{1,m}(t)\cdot N_i(t) + b_{0,m}(t)) \qquad t \in [0,\ T]. \tag{2.72}$$

where we denote by $\mathbb{M}$ the index set of the affine pieces that constitute the piecewise affine function. In addition, we let $b_{1,m}(t)$ and $b_{0,m}(t)$ be the multiplier of the first- and zeroth-order term, respectively, of the m-th affine piece for link I_i. We further denote $\boldsymbol{b}(t) := (b_{\tau,m}(t) :\ \tau \in \{0,1\},\ m \in \mathbb{M})$ at time $t \in [0,\ T]$. Then, we are concerned with the following constraint that, again, the total emission should be bounded from above by a user-specified level even at the worst-case scenarios:

$$\int_0^T \epsilon_i(\boldsymbol{b}(t),\ N_i(t))dt \le E_i \qquad \text{for all } \boldsymbol{b} \in \boldsymbol{\eta}_b \tag{2.73}$$

where the budget uncertainty is employed by denoting

$$\boldsymbol{\eta}_b = \{\boldsymbol{b} :\ L_{\tau,m} \le b_{\tau,m}(t) \le U_{\tau,m},\ \text{for all } \tau \in \{0,1\},\ m \in \mathbb{M},\ \sum_{m\in\mathbb{M}} \int_0^T b_{1,m}(t)\,dt \;\le\; \frac{T\sum_{m\in\mathbb{M}} U_{1,m}}{\sigma}\right\} \tag{2.74}$$

The constraint (2.73) can be immediately discretized as:

$$\max_{m\in\mathbb{M}} \sum_{k=1}^{N} (b_{1,m,k}\cdot N_{i,k} + b_{0,m,k})\delta t \le E_i \qquad \text{for all } \hat{\boldsymbol{b}} \in \hat{\boldsymbol{\eta}}_b,\ t \in [0,\ T]. \tag{2.75}$$

where $\hat{\boldsymbol{b}} := (b_{\tau,m,k} : \ \tau \in \{0,1\},\ m \in \mathbb{M},\ 1 \le k \le N)$ while the discretized uncertainty set is given by:

$$\hat{\boldsymbol{\eta}}_b = \Big\{ \hat{\boldsymbol{b}} : \ L_{\tau,m} \le b_{\tau,m,k} \le U_{\tau,m}, \text{ for all } \tau \in \{0,1\},\ m \in \mathbb{M}, \\ \sum_{m\in\mathbb{M}} \sum_{k=1}^{N} b_{1,m,k}\delta t \ \le \ \frac{T\sum_{m\in\mathbb{M}} U_{1,m}}{\sigma} \Big\} \quad (2.76)$$

The following theorem shows that the robust constraint (2.75) can be equivalently rewritten into a set of linear constraints.

Theorem 2.6. *Let $-\infty < L_{\tau,m} < U_{\tau,m} < \infty$ for all $\tau \in \{0,1\}$ and $m \in \mathbb{M}$. If $\hat{\boldsymbol{\eta}}_b$ has nonempty interior, the semi-infinite constraint (2.75) is equivalent to the following set of constraints:*

$$\sum_{k=1}^{N} U_{1,m}\beta_{k,m} - \sum_{k=1}^{N} L_{1,m}\gamma_{k,m} + \frac{T\sum_{m\in\mathbb{M}} U_{1,m}}{\sigma\delta t}\theta_m + NU_{0,m}\,\delta t \ \le \ E_i \qquad \text{for all } m \in \mathbb{M} \quad (2.77)$$

$$\theta_m + \beta_{k,m} - \gamma_{k,m} \ = \ N_{i,k}\delta t \qquad \text{for all } k = 0,1,...,N,\ m \in \mathbb{M} \quad (2.78)$$

$$\beta_{k,m},\ \gamma_{k,m},\ \theta_m \ \ge \ 0 \qquad \text{for all } k = 0,1,...,N\ m \in \mathbb{M} \quad (2.79)$$

where $\beta_{k,m},\ \gamma_{k,m}$ and θ_m are dummy variables.

Proof. Notice that (2.75) can be immediately rewritten as

$$\max_{\boldsymbol{b}\in\boldsymbol{\eta}_b} \max_{m\in\mathbb{M}} \sum_{k=1}^{N} (b_{1,m,k}\cdot N_{i,k} + b_{0,m,k}) \le E_i \quad (2.80)$$

which, by switching the two "max" operators, is equivalent to

$$\max_{m\in\mathbb{M}} \max_{\boldsymbol{b}\in\boldsymbol{\eta}_b} \sum_{k=1}^{N} (b_{1,m,k}\cdot N_{i,k} + b_{0,m,k}) \le E_i \quad (2.81)$$

Notice that we can represent the above inequality by a set of inequalities:

$$\max_{\boldsymbol{b}\in\boldsymbol{\eta}_b} \sum_{k=1}^{N} (b_{1,m,k}\cdot N_{i,k} + b_{0,m,k}) \le E_i \qquad m \in \mathbb{M}. \quad (2.82)$$

We can then invoke the same duality-based approach as in proving Theorem 2.3 to represent (2.82) by linear constraints:

$$\sum_{k=1}^{N} U_{1,m}\beta_{k,m} - \sum_{k=1}^{N} L_{1,m}\gamma_{k,m} + \frac{T\sum_{m\in\mathbb{M}} U_{1,m}}{\sigma\delta t}\theta_m + NU_{0,m}\,\delta t \ \le \ E_i \qquad \text{for all } m \in \mathbb{M} \quad (2.83)$$

$$\theta_m + \beta_{k,m} - \gamma_{k,m} \ = \ N_{i,k}\delta t \qquad \text{for all } k = 0,1,...,N,\ m \in \mathbb{M} \quad (2.84)$$

$$\beta_{k,m},\ \gamma_{k,m},\ \theta_m \ \ge \ 0 \qquad \text{for all } k = 0,1,...,N\ m \in \mathbb{M} \quad (2.85)$$

where $\beta_{k,m},\ \gamma_{k,m}$ and θ_m are dual variables of the maximization problem involved in the left-hand side of the inequalities (2.82). The above formulation immediately provides the desired result. □

Again, the above theorem provides a computable formulation that preserves linearity even if the relationship between emission rate and vehicle count is captured by a specific type of nonlinear function.

Concave piecewise affine relationship

We will show in the following that when the relationship between the emission rate and the vehicle number becomes concave, as a special case of being nonconvex, we can still maintain the linearity in the constraints by introducing additional integer variables and some modifications to the uncertainty sets.

Specifically, we redefine ϵ_i by

$$\epsilon_i(\boldsymbol{b}(t),\ N_i(t)) := \min_{m\in\mathbb{M}}(b_{1,m}(t)\cdot N_i(t) + b_{0,m}(t)) \qquad t\in[0,\ T]. \tag{2.86}$$

where all other notations remains the same as in subsection 2.3.4. Then, we are interested in the following constraint:

$$\int_0^T \epsilon_i(\boldsymbol{b}(t),\ N_i(t))dt \le E_i \qquad \text{for all } \boldsymbol{b}\in\boldsymbol{\eta}_b,\ t\in[0,\ T] \tag{2.87}$$

where we have a modified uncertainty set $\boldsymbol{\eta}_b$ defined as $\boldsymbol{\eta}_b = \eta_{b,1}\times\eta_{b,2}\times\cdots\times\eta_{b,m}\times\cdots\times\eta_{b,|\mathbb{M}|}$ with

$$\eta_{b,m} = \left\{\boldsymbol{b}_m :\ L_{\tau,m}\le b_{\tau,m}(t)\le U_{\tau,m},\ \text{for all } \tau\in\{0,1\},\ \int_0^T b_{1,m}(t)\,dt\ \le\ \frac{TU_{1,m}}{\sigma_m}\right\}. \tag{2.88}$$

where $\boldsymbol{b}_m := (b_{\tau,m} :\ \tau\in\{0,1\})$. This uncertainty set differentiates from that in the previous subsection in that the uncertain parameters for different pieces of affine functions are uncorrelated, namely, the constraints for the uncertain parameters of different affine pieces in the uncertainty set are decoupled. A natural discretization to this constraint will give us:

$$\min_{m\in\mathbb{M}}\sum_{k=1}^{N}(b_{1,m,k}\cdot N_{i,k} + b_{0,m,k})\delta t \le E_i$$
$$\text{for all } \hat{\boldsymbol{b}} := (\hat{\boldsymbol{b}}_1,\ldots,\hat{\boldsymbol{b}}_{|\mathbb{M}|})\in\hat{\boldsymbol{\eta}} := \hat{\eta}_{b,1}\times\cdots\times\hat{\eta}_{b,|\mathbb{M}|},\ \text{for all } I_i\in\mathbb{I}. \tag{2.89}$$

where $\hat{\boldsymbol{b}}_m := (b_{\tau,m,k} :\ \tau\in\{0,1\},\ 1\le k\le N)$ for any $m\in\mathbb{M}$ and $\hat{\eta}_{b,m}$ is formulated as

$$\hat{\eta}_{b,m} = \left\{\hat{\boldsymbol{b}}_m :\ L_{\tau,m}\le b_{\tau,m,k}\le U_{\tau,m},\ \text{for all } \tau\in\{0,1\},\ \sum_{k=1}^{N} b_{1,m,k}\delta t\ \le\ \frac{TU_{1,m}}{\sigma_m}\right\} \tag{2.90}$$

Evidently, constraint (2.89) is the same as stipulating that

$$\max_{\hat{\boldsymbol{b}}\in\hat{\boldsymbol{\eta}}_b}\min_{m\in\mathbb{M}}\sum_{k=1}^{N}(b_{1,m,k}\cdot N_{i,k} + b_{0,m,k})\delta t \le E_i,\ \text{for all } I_i\in\mathbb{I}. \tag{2.91}$$

Notice that, when we fix a feasible sequence of $\{N_{i,k} :\ 1\le k\le N\}$, the left-hand side of this inequality can be rewritten as:

$$\max_{\hat{\boldsymbol{b}}\in\hat{\boldsymbol{\eta}}_b}\min_{\boldsymbol{\upsilon}\in V}\left\{\sum_{m\in\mathbb{M}}\upsilon_m\sum_{k=1}^{N}(b_{1,m,k}\cdot N_{i,k} + b_{0,m,k})\delta t \doteq \mathcal{F}(\hat{\boldsymbol{b}},\ \boldsymbol{\upsilon})\right\} \tag{2.92}$$

where $V := \{\boldsymbol{\upsilon} = (\upsilon_m : \ m \in \mathbb{M}) \in \mathbb{R}^m : \ \mathbf{1}^\top \boldsymbol{\upsilon} = 1, \ \boldsymbol{\upsilon} \geq 0\}$. Since $\mathcal{F}(\hat{\boldsymbol{b}}, \ \boldsymbol{\upsilon})$ is convex in $\boldsymbol{\upsilon}$ and concave in $\hat{\boldsymbol{b}}$, we can switch the "max" and "min" operator to obtain a dual problem without duality gap, i.e.,

$$\max_{\hat{\boldsymbol{b}} \in \hat{\boldsymbol{\eta}}_b} \min_{\boldsymbol{\upsilon} \in V} \mathcal{F}(\hat{\boldsymbol{b}}, \ \boldsymbol{\upsilon}) = \min_{\boldsymbol{\upsilon} \in V} \max_{\hat{\boldsymbol{b}} \in \hat{\boldsymbol{\eta}}_b} \mathcal{F}(\hat{\boldsymbol{b}}, \ \boldsymbol{\upsilon}) \tag{2.93}$$

for any feasible sequence of $\{N_{i,k} : \ 1 \leq k \leq N\}$. Therefore, constraint (2.89) is equivalently restated as,

$$\min_{\boldsymbol{\upsilon} \in V} \max_{\hat{\boldsymbol{b}} \in \hat{\boldsymbol{\eta}}_b} \mathcal{F}(\hat{\boldsymbol{b}}, \ \boldsymbol{\upsilon}) \leq E_i \qquad \text{for all } I_i \in \mathbb{I}, \tag{2.94}$$

which can be rewritten as, for all I_i:

$$\min_{\boldsymbol{\upsilon} \in V} \max_{\hat{\boldsymbol{b}} \in \hat{\boldsymbol{\eta}}_b} \left\{ \sum_{m \in \mathbb{M}} \upsilon_m \sum_{k=1}^{N} (b_{1,m,k} \cdot N_{i,k} + b_{0,m,k}) \delta t \right\} \tag{2.95}$$

$$= \min_{\boldsymbol{\upsilon} \in V} \max_{\hat{\boldsymbol{b}} \in \hat{\boldsymbol{\eta}}_b} \left\{ \sum_{m \in \mathbb{M}} \upsilon_m \sum_{k=1}^{N} (b_{1,m,k} \cdot N_{i,k} + b_{0,m,k}) \delta t \right\} \tag{2.96}$$

$$= \min_{\boldsymbol{\upsilon} \in V} \left\{ \sum_{m \in \mathbb{M}} \upsilon_m \left[\max_{\hat{\boldsymbol{b}} \in \hat{\boldsymbol{\eta}}_{b,m}} \sum_{k=1}^{N} (b_{1,m,k} \cdot N_{i,k} + b_{0,m,k}) \delta t \right] \right\} \tag{2.97}$$

$$\leq E_i. \tag{2.98}$$

Notice that the second last line above is obtained under the assumption that the uncertainty sets for the parameters of different affine pieces are decoupled. This constraint dictates that a feasible solution to the signal control model should satisfy at least one piece of the affine functions when the uncertain parameter is the most adversarial. Such a constraint can be represented by a set of linear constraints involving "big-M" approach and additional binary variables:

$$\begin{cases} \sum_{k=1}^{N} (b_{1,m,k} \cdot N_{i,k} + b_{0,m,k}) \delta t - \mathcal{M}(1 - z_m) \leq E_i \qquad \text{for all } \hat{\boldsymbol{b}}_m \in \hat{\eta}_{b,m}, \ m \in \mathbb{M} \\ \sum_{m \in \mathbb{M}} z_m = 1 \end{cases} \tag{2.99}$$

where $\mathcal{M} \in \mathbb{R}_+$ is a sufficiently large number. Then, we can again apply the same duality-based procedures as in proving Theorem 2.3 and 2.6 to obtain computable reformulations that maintain linearity.

Theorem 2.7. *Let $-\infty < L_{\tau,m} < U_{\tau,m} < \infty$ for all $\tau \in \{0, 1\}$ and $m \in \mathbb{M}$. If $\hat{\boldsymbol{\eta}}_b$ has nonempty interior, the semi-infinite constraint (2.89) is equivalent to the following set of constraints:*

$$\sum_{k=1}^{N} U_{1,m} \beta_{k,m} - \sum_{k=1}^{N} L_{1,m} \gamma_{k,m} + \frac{T U_{1,m}}{\sigma_m \delta t} \theta_m + N U_{0,m} \, \delta t - \mathcal{M}(1 - z_m) \ \leq \ E_i \qquad \text{for all } m \in \mathbb{M} \tag{2.100}$$

$$\sum_{m \in \mathbb{M}} z_m = 1 \tag{2.101}$$

$$\theta_m + \beta_{k,m} - \gamma_{k,m} \ = \ N_{i,k} \delta t \qquad \text{for all } k = 0, 1, ..., N, \ m \in \mathbb{M} \tag{2.102}$$

$$\beta_{k,m}, \ \gamma_{k,m}, \ \theta_m \ \geq \ 0 \qquad \text{for all } k = 0, 1, ..., N, \ m \in \mathbb{M} \tag{2.103}$$

where $\beta_{k,m}$, $\gamma_{k,m}$ and θ_m are dummy variables.

Remark 2.8. *The concave piecewise affine relationship results in nonconvex constraints, which can generate a substantial computational challenge. In fact, those constraints cannot be well handled by the existing commercial solvers, including CPLEX and Gurobi. Nonetheless, with the above theorem, we can again retain linearity by introducing additional integer variables. Further notice that due to constraint* (2.101)*, these integer variables are highly correlated so that the search space of the problem grows only by a scale of* $|\mathbb{M}|$*. Therefore, our reformulation significantly reduces the computational ramifications of handling a set of nonconvex constraints.*

2.3.5 Some Discussions in Modeling Generalization

As mentioned in the introduction, the model can be easily extended to capture two other different scenarios that are of application importance: (1) when the differences between link emissions is to be constrained, i.e., the so called equity constraint; and (2) when the total emission amount of all links is to be minimized.

2.4 Equity Constraints

The equity constraint might occur when the planner of the traffic system would like to enforce emissions to be distributed evenly across all the links in a network. To capture this enforcement, we consider the following constraint:

$$\int_0^T \epsilon_i(\boldsymbol{a},\ N_i(t))dt - \int_0^T \epsilon_j(\boldsymbol{a},\ N_j(t))dt \leq E_{ij} \qquad \text{for all } I_i \in \mathbb{I},\ I_j, \tag{2.104}$$

where, for now, we assume no uncertainty in the parameters $\boldsymbol{a}_i$ and $\boldsymbol{a}_j$. By stipulating an affine relationship between emission rate and vehicle number, this constraint can be immediately rewritten into

$$\int_0^T \left\{a_1(t)\left[(N_{up,i}(t) - N_{down,i}(t)) - (N_{up,j}(t) - N_{down,j}(t))\right] + a_0(t)\right\} dt \leq E_{ij} \qquad \text{for all } I_i \in \mathbb{I},\ I_j, \tag{2.105}$$

If ϵ_i and ϵ_j are given as affine functions, the same set of arguments as in Theorem 2.3 can be immediately extended to handle the equality constraint. Now, we allow $\boldsymbol{a}(t)$ to be uncertain and the uncertainty is constrained within the budget uncertainty set (2.49). Then the robust constraint

$$\int_0^T \left\{a_1(t)\left[(N_{up,i}(t) - N_{down,i}(t)) - (N_{up,j}(t) - N_{down,j}(t))\right] + a_0(t)\right\} dt \leq E_{ij} \qquad \text{for all } \boldsymbol{a}(t) \in \boldsymbol{\eta}_a,\ \text{for all } I_i \in \mathbb{I},\ I_j, \tag{2.106}$$

becomes immediately a special case of (2.46).

2.4.1 Minimizing emission-related criteria

The proposed model is also easily extendable to the case where the emission criteria are disutilities to be minimized. In such a case, we will invoke the "epigraph reformulation." For example, if the objective is to minimize the total emission amount on a certain link I_i with I_i, instead of minimizing $\int_0^T \epsilon_i(\boldsymbol{a}, N_i(t))dt$, we can minimize a dummy variable z with one additional constraint for the feasible region $\int_0^T \epsilon_i(\boldsymbol{a}, N_i(t))dt \leq z$. This additional constraint conforms with (2.46).

Combining the above observation with subsection 2.4, we see the proposed model also applies to the case where the difference among the emission amount (equity) of different links is to be minimized (maximized).

2.5 Numerical Study

2.5.1 Network setup

In this section, we consider a hypothetical network consisting of four intersections, three of which are signalized; see Figure 4. The ten links in the network have the same triangular fundamental diagram, whose parameters are shown in Table 1. In addition, all links have the same length of 400 meters. For simplicity, we assume that routing is such that vehicles at all intersections have a fixed probability of selecting either of the two downstream approaches, and the turning ratios are specified as follows.

$$\alpha_{1,5} = 0.50, \qquad \alpha_{3,5} = 0.40, \qquad \alpha_{2,6} = 0.30, \qquad \alpha_{5,6} = 0.50, \qquad \alpha_{10,3} = 0.53$$

Note that this assumption is not essential to our formulation or computation, but was made to simplify the presentation of results. The time horizon of our numerical example is a 15-minute time period, with a time step of 10 seconds.

In order to test the effectiveness of the proposed signal timing in reducing both congestion and emission under different levels of network loads, we consider three scenarios with three different demand profiles at the upstream end of all boundary links. The demand profile in the first scenario, which is shown in Figure 4, corresponds to the lightest traffic load. For the second and third demand profiles, we uniformly increase all the boundary flows in the first scenario by a constant. Table 2 shows the ratios of boundary flows and the link flow capacity.

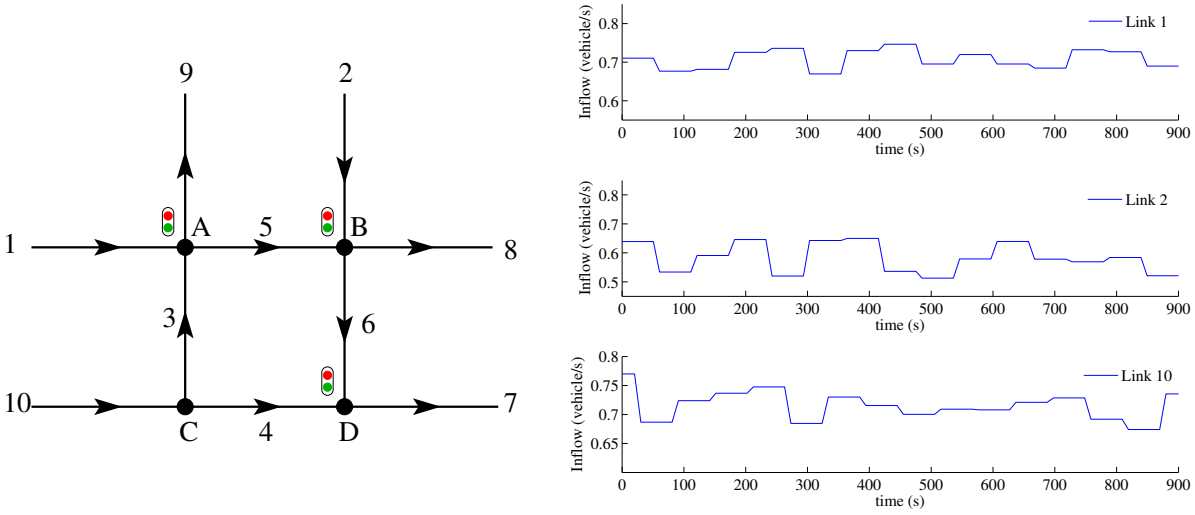

Figure 4: Test network (left); and the demand profile corresponding to Scenario I (right).

	Free-flow speed (meter/second)	Jam density (vehicle/meter)	Critical density (vehicle/meter)	Flow capacity (vehicle/second)
Triangular fd	40/3	0.4	0.1	4/3

Table 1: Link parameters. The fundamental diagram is triangular.

	Scenario I (light)	Scenario II (medium)	Scenario III (heavy)
Link 1	53.1 %	60.6 %	64.4 %
Link 2	43.7 %	51.2 %	54.9 %
Link 10	51.6 %	68.4 %	83.38 %

Table 2: Demand profiles in the three scenarios with different traffic loads. The values in the table represent ratios of the average boundary flow and the flow capacity.

2.5.2 Calibrating the macroscopic relationship

The macroscopic relationship between the emission rate at a link level and the occupancy of the link is specific to the type and characteristics of each link, and may be sensitive to link flow profile, signal control, etc. Therefore, we need to identify this relationship using simulation and curve-fitting. To determine this relationship for our numerical experiments, we employ the modal emission model discussed in Section 2.2.2. This model was selected because it had a higher degree of uncertainty; using the average speed model should provide even better results. The process described in Section 2.2 was repeated to determine the aggregate emissions rate for each link. Again, this process included the random generation of binary variables to simulate the impact of traffic signals and the resulting stop-and-go waves that they would create along the link. Note that we perform this process here for a single link, noting that the other links are identical.

The simulation contains $42,000$ samples, all of which are plotted in Figure 5. The macroscopic relationship is approximately affine with the following regression coefficients

$$AER \;=\; a_1 \times LO + a_0 \;=\; 52.31 \times LO + 318.63 \tag{2.107}$$

with an R^2 value of 0.9794, where AER (in grams/hour) denotes the aggregated emission rate of hydrocarbon on a link level; LO (in number of vehicles) denotes the link occupancy.

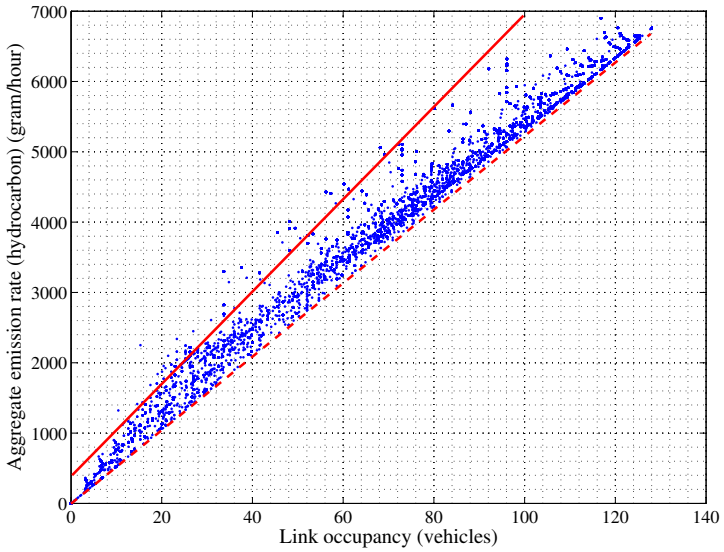

Figure 5: Scatter plot of sample points from simulation. The solid line represents the upper envelope of the uncertainty region; the dashed line represent the lower envelope of the uncertainty region.

The high R^2 value indicates that we can indeed approximate this macroscopic relationship with

an affine model. In order to construct the uncertainty set of the form (2.68) for the robust optimization counterpart, we select the following lower and upper bounds for the affine coefficients:

$$L_1 \ \leq \ a_1 \ \leq \ U_1, \qquad L_0 \ \leq \ a_0 \ \leq \ U_0 \tag{2.108}$$

where

$$L_0 = 0, \quad U_0 = 400, \quad L_1 = 53.3, \quad U_1 = 66 \tag{2.109}$$

The corresponding lower envelope (by letting $a_1 = 53.3$, $a_0 = 0$) and upper envelope (by letting $a_1 = 66$, $a_0 = 400$) of the uncertain region are now shown in Figure 5. Notice that one has a lot of freedom in choosing these upper and lower bounds; however, they do affect the performance of the resulting RO program. As we commented in Section 2.3.3, the upper envelope set a worse-case value for the emission rates, and it is likely to overestimate the emission rates for some/most scenarios. From Figure 5 we see that while the upper envelope provides a tight bound on the emission rates when the traffic is relatively light (i.e., $0 \leq LO \leq 40$ vehicles), it tends to mostly overestimate the emission rates when the traffic volume grows (i.e., $LO \geq 40$ vehicles). To avoid the robust constraints being too conservative, we invoke the parameter σ introduced in (2.68) to adjust the conservativeness by allowing some realized coefficients $a_{1,k}$ to be strictly less than the upper bound U_1, that is,

$$\sum_{k=1}^{N} a_{1,k} \ \leq \ N\frac{U_1}{\sigma} \qquad \text{for some } \ \sigma \in \left[1, \ \frac{U_1}{L_1}\right] \tag{2.110}$$

where $a_{1,k}$ can be interpreted as the first-order coefficient in an actual (realized) instance of the relationship between LO_k and AER_k; here the subscript k indicates the *k-th* time step. A general rule of thumb is that the more the upper bound seems to overestimate, the larger σ should be, although ideally such choice should be specifically quantified and even optimized based on available data. The interested reader is referred to Bandi and Bertismas (2012) and Bertsimas et al. (2014) for some discussions on data-driven calibration of the uncertainty set. In our particular example, we choose $\sigma = 1.2$. Other choices of σ could also be considered but will not be elaborated in this report.

Notice that the region formed by the lower and upper envelopes does not contain all sample points. However, the majority (96.06%) of these points fall within this region, and we treat the rest as outliers. The reason is that these outliers, which make up just 3.94% of the total estimates, are sparsely distributed outside (and consistently above) the uncertainty region. Including these values within our uncertainty set would make our estimation too conservative by considering the (very small) chance that these emission rates occur.

The uncertainty set for the robust optimization, according to (2.68), is therefore constructed as follows.

$$\hat{\eta}_{a,i} = \left\{ (a_{0,k}, \, a_{1,k}) : 0 \leq a_{0,k} \leq 400, \ 53.3 \leq a_{1,k} \leq 66, \ \text{for all } 1 \leq k \leq N, \ \sum_{k=1}^{N} a_{1,k} \leq 55N \right\} \tag{2.111}$$

for all link $I_i \in \mathbb{I}$ in the network. By virtue of Corollary 2.5, the above semi-infinite constraint set transforms to a finite set of linear constraints, which are part of a mixed-integer linear program.

2.5.3 The base case

For comparison purposes, we first consider a base case where the traffic signal timing is optimized, without any emission considerations. This is achieved by simply solving the mixed-integer linear program introduced in Section 2.1.5, namely, with constraints (2.27)-(2.30) and (2.32)-(2.35). Since

the base case is mainly concerned with maximizing network throughput and minimizing delays, we adopt the following form for the objective function.

$$\max \sum_{k=1}^{N} \frac{1}{1+k} \left(\hat{q}_7^k + \hat{q}_8^k + \hat{q}_9^k \right) \tag{2.112}$$

where $\hat{q}_7^i$, $\hat{q}_8^i$ and $\hat{q}_9^i$ are the exit flows at the i-th time step on links 7, 8, and 9, respectively. An objective function of the form (2.112) tends to maximize the network throughput at any instance of time, and is commonly employed in the literature on network optimization (Han et al., 2013, 2014a,b).

Scenario I	Objective value	5.331					
	HC emissions (gram)	link 1	link 2	link 3	link 4	link 5	link 6
		390.5	309.1	208.6	158.7	343.4	210.2
	Total emission	1620.5 (gram)					

Scenario II	Objective value	6.615					
	HC emissions (gram)	link 1	link 2	link 3	link 4	link 5	link 6
		558.0	400.4	263.5	214.3	514.8	252.9
	Total emission	2203.9 (gram)					

Scenario III	Objective value	7.142					
	HC emissions (gram)	link 1	link 2	link 3	link 4	link 5	link 6
		1359.2	430.6	560.1	269.1	553.0	252.7
	Total emission	3424.7 (gram)					

Table 3: Objective value and hydrocarbon (HC) emissions in the base case. Three scenarios with three different demand profiles are considered. The objective value measures the throughput of the network and is calculated from expression (2.112).

The results of the base case corresponding to three demand profiles are summarized in Table 3[2]. The results also include a hydrocarbon emission amount on each link, which is calculated from the resulting link flows and the detailed modal emission model elaborated in Section 2.2.2. The purpose of this table is two-fold: (1) to enable the comparison with the emission-constrained results presented later, and (2) to suggest appropriate upper bounds on the emission amount for the robust optimization. In presenting our results, we only consider links 1 through 6, since the rest of the links are not directly controlled by the signals under consideration.

2.5.4 Simultaneous control of traffic and emission of hydrocarbon

In this subsection, we solve the signal optimization problem with emission side constraints; such problem is referred to as an LWR-E problem. This is achieved by solving the MILP for the base case with additional emission-related robust counterpart expressed by (2.68)-(2.70), where the values selected for the lower and upper bounds are presented in (2.108)-(2.109). In view of the base case summarized in Table 3, we chose the following upper bounds (in grams) on the emission amount for each link, where bounds strictly below the corresponding emissions in the base case are highlighted

[2]Throughout this numerical study, the MILPs were solved with ILOG Cplex 12.1.0, which ran with Intel Xeon X5675 Six-Core 3.06 GHz processor provided by the Penn State Research Computing and Cyberinfrastructure.

in boldface.

Scenario I: $E_1 = \mathbf{390}$, $E_2 = 310$, $E_3 = 210$, $E_4 = 160$, $E_5 = \mathbf{310}$, $E_6 = 240$
Scenario II: $E_1 = 600$, $E_2 = \mathbf{380}$, $E_3 = 300$, $E_4 = \mathbf{210}$, $E_5 = \mathbf{490}$, $E_6 = \mathbf{250}$
Scenario III: $E_1 = \mathbf{1100}$, $E_2 = \mathbf{440}$, $E_3 = 750$, $E_4 = 300$, $E_5 = 600$, $E_6 = 300$

Notice that we did not set all the bounds to be strictly below the actual emissions in the base case. This is because all the links in the network are in conflict with one another in the sense that releasing vehicles from one approach will block the vehicles in the conflicting approach to the same intersection. Thus any signal control strategy is unlikely to simultaneously reduce the emission on all links. In fact, setting the bounds to be strictly below the actual emissions in the base case leads to infeasible problems in most of our calculations.

Scenario I	Objective value	5.330 **(0.02% less than the base case)**					
	HC emissions (grams) (upper bound)	link 1	link 2	link 3	link 4	link 5	link 6
		390.2 (390)	313.3 (310)	204.8 (210)	161.3 (160)	289.8 (310)	229.0 (240)
	Total emission	1588.4 grams **(1.98% less than the base case)**					

Scenario II	Objective value	6.612 **(0.05% less than the base case)**					
	HC emissions (grams) (upper bound)	link 1	link 2	link 3	link 4	link 5	link 6
		598.5 (600)	369.2 (380)	303.8 (300)	214.6 (210)	443.8 (490)	247.1 (250)
	Total emission	2157.0 grams **(2.12% less than the base case)**					

Scenario III	Objective value	7.058 **(1.18% less than the base case)**					
	HC emissions (grams) (upper bound)	link 1	link 2	link 3	link 4	link 5	link 6
		1160.5 (1100)	434.6 (440)	756.4 (750)	272.1 (300)	622.2 (600)	294.5 (300)
	Total emission	3540.3 grams **(3.38% more than the base case)**					

Table 4: Objective value and hydrocarbon (HC) emissions in the LWR-E case.

The results of the proposed MILP formulation for the emission-constrained signal optimization are summarized in Table 4. We see that for all three scenarios, our proposed signal optimization scheme effectively keeps the emissions below the prescribed level, and this is done at a relatively small cost to the overall throughput of the network; that is, compared with the base case, the objective values in the LWR-E case decrease by only 0.02%, 0.05%, and 1.18% in Scenarios I, II, and III, respectively.[3] In addition, for Scenarios I and II, bounding the emission amount on certain links successfully reduces the total emission on the entire network by 1.98% and 2.12%, respectively.

In Scenario 3, where the traffic load becomes heavy, we observe that a local reduction of emission (on link 1 where emission has been reduced from 1359 grams to 1160 grams) results in an overall increase in the total emission on the network. Moreover, the total network throughput suffers more than the previous two scenarios. Such a Braess-like paradox is understandable in that an improvement on a single link will inevitably affect adjacent links, and such effect may propagate through the network in a highly nonlinear way if the traffic load is heavy. This phenomenon thus

[3]Recall that while lower total emissions are desired, the objective function is such that a lower value represents a worse scenario.

calls for a well-balanced and/or multi-objective optimization of signalized networks with emission considerations. A visualization of the emission profiles for all test scenarios is provided in Figure 6.

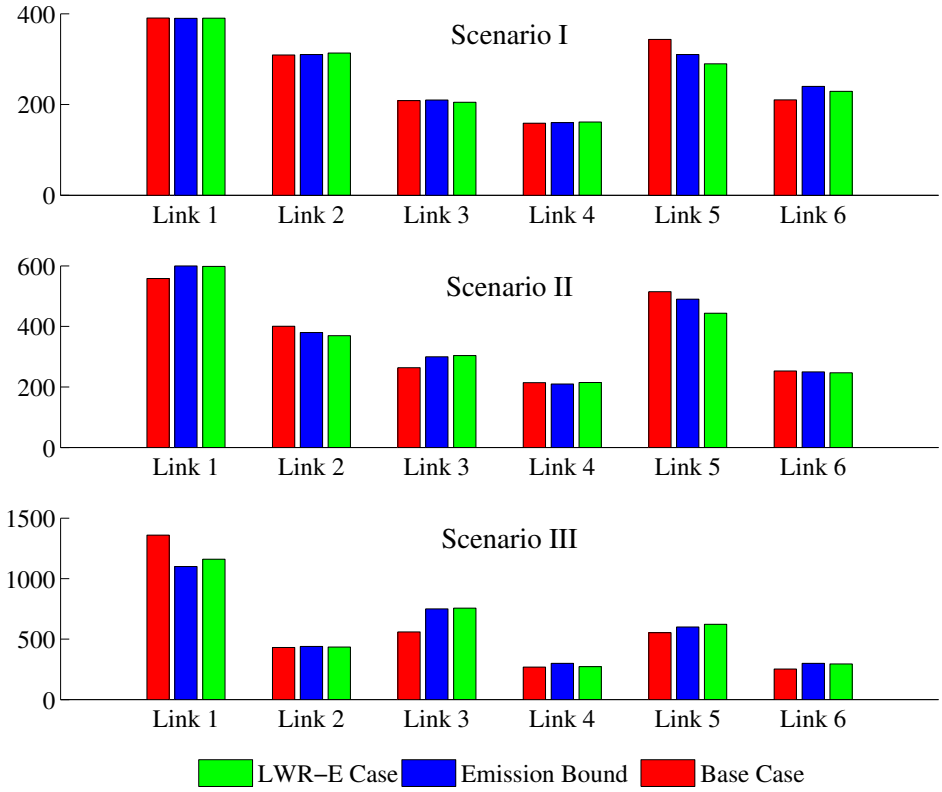

Figure 6: Comparisons of link-specific HC emissions in the base cases and the emission-constrained (LWR-E) cases.

We also see from Table 4 that a few emission constraints are slightly violated; this is expected by the nature of our formulation: 1) in the calibration of the macroscopic relationship in Section 2.5.2, a few data points that lie outside the uncertainty region are not accounted for in our formulation; 2) we chose the parameter σ to be larger than 1 (see (2.110)), which means that the approach taken to handle the uncertainty in the AER is relatively less conservative and could lead to, with a small probability, violation of the constraints. We present a quantification of the violations in Table 5 for all the links in all three scenarios, which ensures that the violations of the constraints are within an acceptable range.

	link 1	link 2	link 3	link 4	link 5	link 6
Scenario I	0.05%	1.06%	-	0.81%	-	-
Scenario II	-	-	1.27%	2.19%	-	-
Scenario III	5.45%	-	0.85%	-	3.70%	-

Table 5: Violations of the emission constraints. "-" means that the actual emission is below the bound.

In order to further analyze emissions mechanism and the ability of traffic signal control to reduce overall emissions, we will look at a particular intersection, which is Node B (see Figure 4)

from Scenario II. In order to enable a visualization of the congestion and emissions on links 2 and 5 connected to Node B, we compute their respective Moskowitz functions $N_2(t, x)$ and $N_5(t, x)$ for both the base case and the LWR-E case. These functions are presented in Figure 7. The surface of each Moskowitz function is separated by a clear shock wave into two domains: the uncongested region and the congested region. The separating shock wave travels back and forth as a result of constantly changing downstream boundary conditions caused by the signal control. We can also observe the time-varying queue lengths near the intersection. From Figure 7 we see that the separating shocks on link 2 in both the base case and the LWR-E case stay closely to the exits (left boundaries) of the links, indicating that link 2 is mostly in the free-flow phase. On the other hand, link 5 in both the base case and the LWR-E case is more congested.

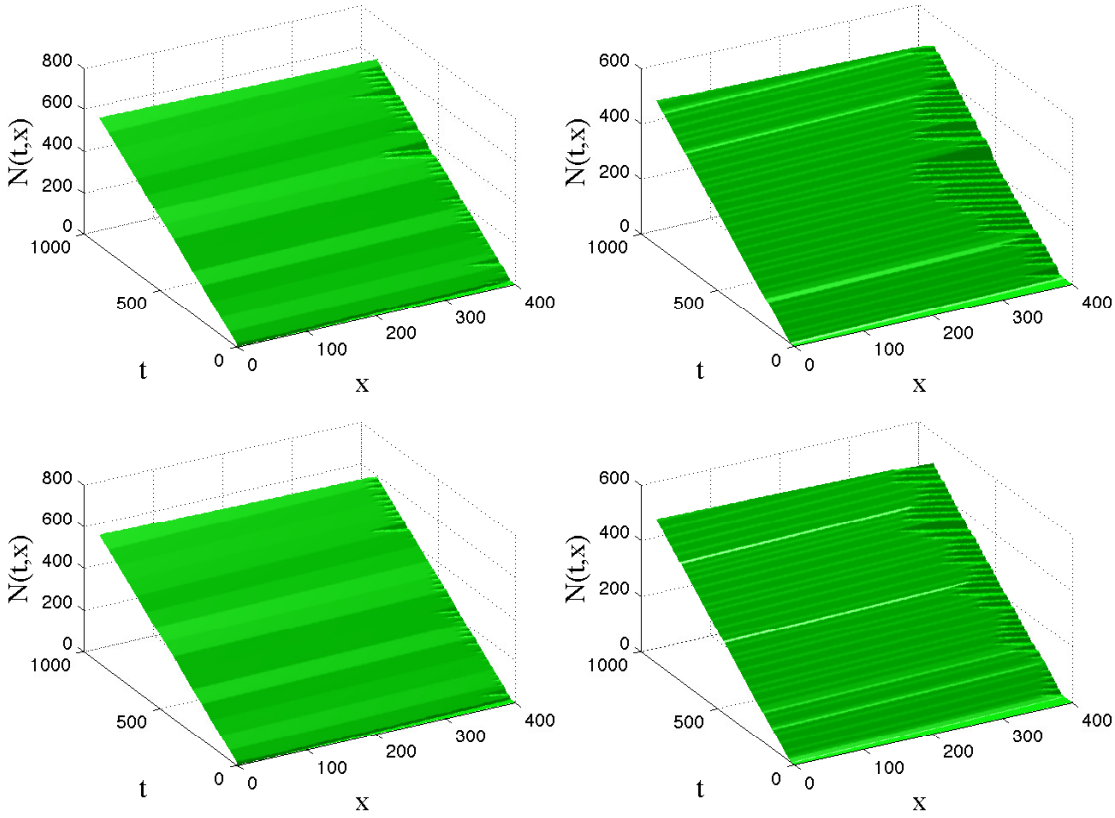

Figure 7: The Moskowitz functions of link 3 in the base case (left) and the LWR-E case (right).

Since the Moskowitz functions $N_2(t, x)$ and $N_5(t, x)$ represent the Lagrangian labels of vehicles passing through location x at time t, its contour lines should represent the spatial-temporal trajectories of moving particles. In order to better observe the stop-and-go waves near the intersection, we present in Figure 8 the contour lines of the Moskowitz functions in the base case and the LWR-E case. We see that, for both link 2 and link 5, the LWR-E case has fewer vehicle stops than the base case. To confirm this, we perform the following simple calculation: the number of stops (represented by the vertical line segments in the figures) in the base case is roughly 17 (link 2) and 76 (link 5), while the number of stops in the LWR-E case is roughly 5 (link 2) and 52 (link 5). Given that there are 50 contour lines in each figure, we estimate that the average number of stops per vehicle is 0.34 (link 2) and 1.52 (link 5) in the base case, and 0.1 (link 2) and 1.04 (link 5) in the LWR-E case. The total emission in the LWR-E case is thus reduced as vehicle stops and acceleration/deceleration

associated has been reduced by the signal controls.

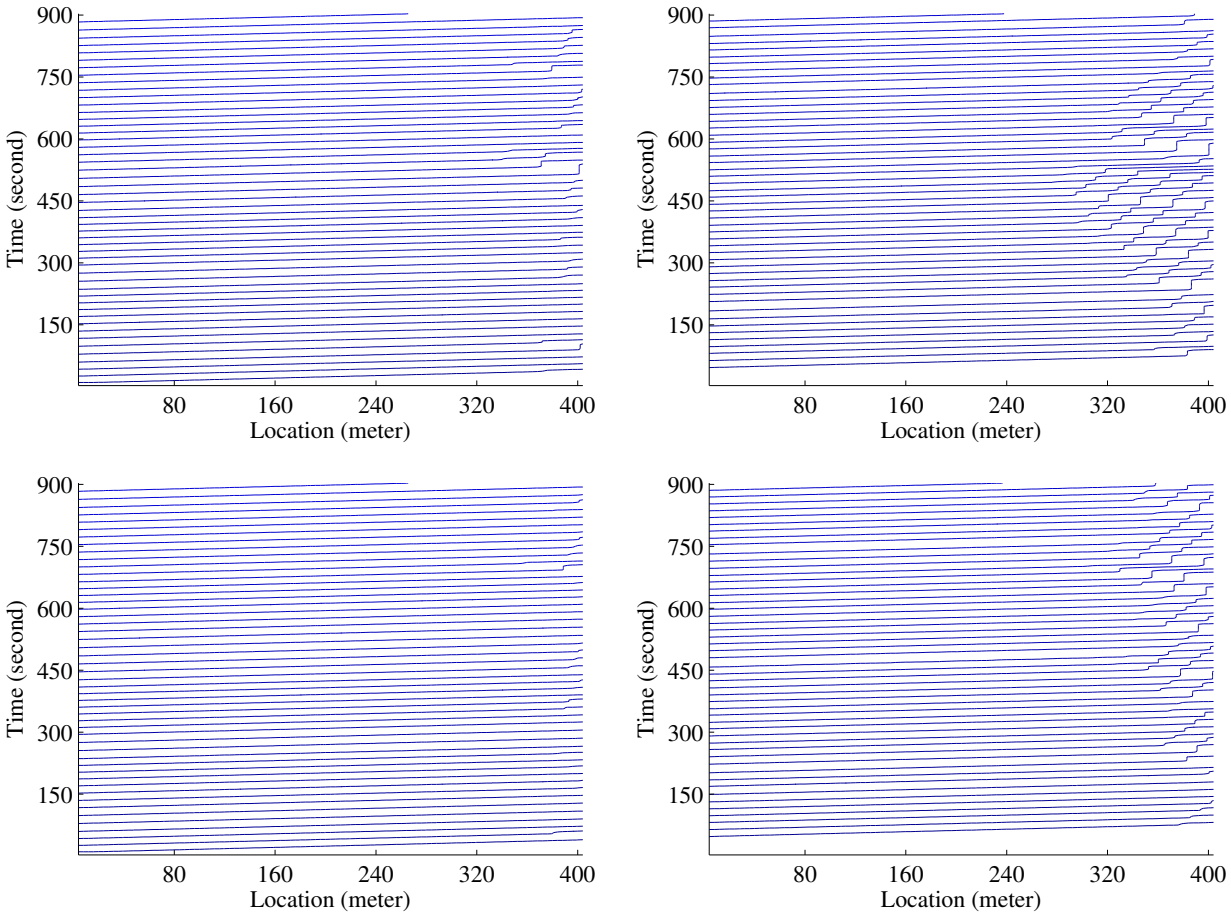

Figure 8: Contour lines of the Moskowitz functions of link 2 (left column) and link 5 (right column), in the base case (top row) and the LWR-E case (bottom row).

2.6 Conclusion

This project proposes a novel robust optimization approach to address emission-related side constraints, in the formulation of a link-based mathematical programming problem for traffic signal control. We take advantage of an empirical relationship between the aggregated emission rate and the link occupancy, and treat the error as modeling uncertainty, which is then handled by the RO technique. Such a computational apparatus turns the otherwise non-convex emission side constraints into explicit and tractable forms.

Further research is underway to (1) validate the linear or polynomial relationships among certain macroscopic traffic quantities, from both statistical and analytical points of view; (2) reveal additional correlations between aggregated emission rate and certain traffic quantities that may facilitate the computational efficiency and tractability of the math programs; and (3) develop heuristic algorithms and computational paradigms for real-time and large-scale deployment.

3 Dynamic Congestion and Tolls with Mobile Source Emission

3.1 Literature Review

3.1.1 Congestion Toll Pricing

The idea of employing toll pricing to mitigate both emission and congestion derives from congestion pricing strategy in Pigou (1920). In the literature, toll pricing problems can be classified into two categories: (1) first-best toll pricing (Arnott and Small, 1994; Hearn and Ramana, 1998; Dial, 1999; 2000), which tolls every arc in the network; and (2) second-best toll pricing (Lawphongpanich and Hearn, 2004), which assumes that only a subset of the arcs is tolled for political or other reasons. However, the literature above focused on toll pricing in static models (see a comprehensive review for static road pricing in Yang and Huang, 2005), which considered only the route choice decisions by the traffic agents, as noted by Yao et al. (2012). A more comprehensive and realistic model ought to take into account the time-dependent nature of traffic flow and dynamic toll pricing. Dynamic congestion pricing in bottleneck models were investigated by Arnott et al. (1990), Arnott and Kraus (1998), Braid (1996) and De Palma and Lindsey (2000). Based on link-delay model (Friesz et al. 1993, 2011), Friesz et al. (2007) proposed an MPEC model and a solution approach to determine the optimal second-best tolling strategy. Yao et al. (2012) further studied a dynamic congestion pricing problem with demand uncertainty. A more comprehensive review on the existing dynamic congestion pricing models and solution approaches was presented in Yao et al. (2012).

The above literature provided evidence for the effectiveness of tolling strategies to stimulate and optimize a traffic network. In this project, we seek to further exploit such a strategy to minimize both traffic congestion and automobile-induced emission simultaneously. To do this, we provide a multiobjective MPEC model of a second-best tolling strategy to determine the optimal toll price. Such an MPEC model incorporates the LWR-Lax model proposed by Friesz et al. (2012) to capture time-varying traffic behaviors. To the best of our knowledge, this is the first attempt to employ tolling to mitigate overall emission in the traffic network, the first dynamic toll pricing model that builds on LWR-Lax model in Friesz et al. (2012), and the first successful integration of LWR-Lax model with mobile source emission model.

3.1.2 Dynamic User Equilibrium Model

In this project, we employ the simultaneous route and departure time-choice DUE model proposed originally by Friesz et al. (1993). For the user equilibrium, unit travel cost, including early and late

arrival penalties, is identical for those route and departure time choices selected by travelers between a given origin-destination pair. Such problem was articulated and formulated as a *variational inequality* (VI) in Firesz et al. (1993). The DUE model typically consists of two major components: the VI formulation of equilibrium constraints and the network performance model known as the *dynamic network loading* (DNL) sub-problem. The DNL aims at describing and predicting time evolution of system states by introducing dynamics to the traffic flows throughout the network. It determines the delay operator which is a key component of the DUE model. The DUE model is intertwined with the determination of path delay and thus the DNL.

Friesz et al. (2001) studied the DUE as a single-level problem by formulating it as a controlled variational inequality. The DNL with *link delay model* (Friesz et al. 1993) and the route/departure time choice were solved simultaneously. In addition, the necessary conditions for optimal control problems with state-dependent time lags were derived. In Friesz and Mookherjee (2006), the theory of optimal control and the theory of infinite dimensional VIs were combined to create an implicit fixed point algorithm for calculating DUE. Friesz et al. (2011) extended the DUE problem from within-day time scale to a day-to-day time scale and formulated the dual time scale DUE problems. In Friesz et al. (2012), the Lighthill-Whitham-Richards model (Lighthill and Whitham 1955; Richards 1956) was employed in the DNL sub-problem, which was then formulated as a system of *differential algebraic equations* (DAEs) using the Lax-Hopf formula (Lax 1957; Evans 2010). The DUE problem was solved efficiently on reasonable size networks (Sioux Falls) with a realistic number of origin-destination pairs and paths.

3.1.3 Mobile Source Emission Models

Modeling approaches of mobile source emission can be classified into three categories: microscopic, macroscopic, and mesoscopic approaches. The microscopic emission models are relatively accurate: they characterize the emission rate on the level of a single vehicle, based on the physical attributes of the vehicle, driving behavior of the driver, as well as the surrounding environment. It is assumed that the rate of emission $e(t)$ of a car can be expressed as a function of instantaneous velocity $v(t)$ and acceleration $a(t)$,

$$e(t) \;=\; f_1\big(v(t),\, a(t)\big). \tag{3.113}$$

Such models can be easily calibrated and validated in the lab. There are several models based on microscopic emission (Barth et al. 1996; Panis et al. 2006; Rakha et al. 2004). The drawback of the microscopic modeling approach is the lack of measurement associated with each individual car's dynamic. On the other hand, it is relatively easy to measure the traffic dynamics on a macroscopic level. The macroscopic emission models (Ekström et al. 2004) express the average emission rate $\bar{e}(t)$ on a road segment as a function of the average density $\bar{\rho}$ and average velocity $\bar{v}(t)$ in that same segment

$$\bar{e}(t) \;=\; f_2\big(\bar{\rho}(t),\, \bar{v}(t)\big) \tag{3.114}$$

The drawback of the macroscopic modeling approaches for emission lies in the fact that the model is difficult to calibrate and validate, due to the lack of measurement of emission rate on a road. The third type of emission models, the mesoscopic emission model, approximates individual vehicles' dynamics using macroscopic flow models and measurements. Then the total emission rate is the aggregation of emission rates on a microscopic level, given by (3.113). The mesoscopic models (Csikós et al. 2011; Csikós and Varga 2011; Zegeye et al. 2010) take the modeling advantages of both macroscopic traffic flow models and microscopic emission models, thus overcome the drawbacks of the previous two approaches.

In this project, we employ the mesoscopic point of view for emission estimation and prediction on a vehicular network. The emission estimation will be embedded in the Dynamic Network Loading

sub-problem, which describes and predicts macroscopic traffic variables given established path flows. The DNL provides a basis for the comparison of various microscopic emission functions, among which we distinguish between the two-argument functions $e(t) = f_1\big(v(t),\, a(t)\big)$ and the single-argument functions $e(t) = f_3\big(v(t)\big)$.

The two-argument functions, such as the one proposed in the Modal emission model (Barth et al. 1996), use a physical approach that associates the power demand function to the various driving conditions of the car such as low/high speed motion, acceleration, stop-and-go, etc. The emission and fuel consumption functions are then expressed as affine functions of the power demand. Such model is very accurate, and can account for vehicles of different types. However, it is relatively difficult to integrate the modal model into macroscopic traffic flow models. In particular, the higher-order traffic quantities such as acceleration cannot be sufficiently captured by first order models such as the Lighthill-Whitham-Richards conservation law (Lighthill and Whitham 1955; Richards 1956); see Section 3.4.1 for more discussion.

The one-argument emission functions on the other hand, usually rely on the average speed. In Rose et al. (1965), it was shown that when a vehicle's travel speed is under $80 km/hour$, the relation between speed v (km/hour) and HC/CO emissions e_x (pound/km) can be approximated by (for now and sequel, e_x denote the emission per unit distance).

$$e_x \;=\; b_1\, v^{-b_2} \tag{3.115}$$

where b_1, b_2 are parameters depending on vehicle type and surrounding environment. Kent and Mudford (1979) collected driving pattern data in Sydney and found that NO_y emission $\tilde{e}_x$ can be modeled by

$$\tilde{e}_x \;=\; \tilde{b}_1 + \frac{\tilde{b}_2}{v} \tag{3.116}$$

According to the Emission Factor Model 2000 (CARB 2000) by California Air Resources Board, constantly updated since 1988, the hot running emissions per unit distance

$$\hat{e}_x \;=\; \text{BER} \times \exp\Big\{\hat{b}_1(v - 17.03) + \hat{b}_2(v - 17.03)^2\Big\} \tag{3.117}$$

where BER stands for basic emission rates, which are constants associated with CO, NO_y, HC. The unit of velocity is $miles/hour$, the unit of $\hat{e}_x$ is $grams/mile$.

3.2 Numerical Techniques for MPEC

MPECs, with its bi-level nature, often create computational difficulty. A common approach to compute an MPEC is to formulate the bi-level program into a *mathematical program with complementarity constraints* (MPCC) (see examples in Ban et al., 2006, and Friesz, 2010). However, as noted in Rodrigues and Monteiro (2006) and in Ban et al. (2006), the complementarity constraints might lose certain constraint qualifications. To resolve this issue, some regularization techniques were proposed. Ralph and Wright (2003) studied a relaxation approach, which was applied by Ban et al. (2006) to solve a continuous network design problem. Anitescu (2000) proposed a l_1-penalty approach and studied its impact on the convergence of an interior point algorithm, while Monteiro and Meira (2011) tested a quadratic penalty function. According to their numerical results, quadratic penalty was a promising approach to handle complementarity constraints. However, discussions above all focused on MPCC in the context of finite dimensional programs. As for a continuous time dynamic MPEC, numerical techniques were scarcely visited, except for a single-level reformuation of Friesz et al. (2007), a metaheuristic approach in Yao et al. (2012) and a simultaneous discretization-based method in Raghunathan (2004).

In this project, we utilize the quadratic penalty method to solve our dynamic MPEC model. In specific, we relax the model by dropping the complementarity constraints and attaching to the objective function a quadratic penalty function for the dropped constraints. Our numerical tests generate positive results.

3.3 Dynamic User Equilibrium

In this section, we will briefly review the DUE problem which serves as the lower-level component of our MPEC formulation. The proposed DUE model was formulated as a variational inequality (Friesz et al. 1993) and a differential variational inequality (Friesz and Mookherjee 2006), then solved via a fixed-point algorithm in Hilbert space (Friesz et al. 2011).

3.3.1 The DUE formulation

Consider a planning horizon $[t_0,\, t_f] \subset \Re_+$. The most crucial ingredient of a dynamic user equilibrium model is the path delay operator, which provides the delay on any path p per unit of flow departing from the origin of that path; it is denoted by

$$D_p(t,h) \quad \text{for all } p \in \mathcal{P}$$

where $\mathcal{P}$ is the set of all paths employed by travelers, t denotes departure time, and h is a vector of departure rates. The path delay operators are obtained from the DNL procedure by summing up arc delays along the path. From these we construct effective unit path delay operators

$$\Psi_p(t,h) = D_p(t,h) + F\left[t + D_p(t,h) - T_A\right] \quad \text{for all } p \in \mathcal{P} \tag{3.118}$$

where T_A is the desired arrival time. Introducing the fixed trip matrix $\left(Q_{ij} : (i,\, j) \in \mathcal{W}\right)$, where each $Q_{ij} \in \Re_+$ is the fixed travel demand, expressed as a volume, between origin-destination pair $(i,j) \in \mathcal{W}$ and $\mathcal{W}$ is the set of all origin-destination pairs. Additionally, we will define the set $\mathcal{P}_{ij}$ to be the subset of paths that connect origin-destination pair $(i,j) \in \mathcal{W}$.

Denote the set of path flows $h = \{h_p : p \in \mathcal{P}\}$, we stipulate that path flows are square integrable:

$$h \in \left(\mathcal{L}^2_+[t_0,\, t_f]\right)^{|\mathcal{P}|}$$

We define the set of feasible flows by

$$\Lambda_0 = \left\{ h \geq 0 : \sum_{p \in \mathcal{P}_{ij}} \int_{t_0}^{t_f} h_p\left(t\right) dt = Q_{ij} \quad \text{for all } \ (i,j) \in \mathcal{W} \right\} \subseteq \left(L^2_+\left[t_0, t_f\right]\right)^{|\mathcal{P}|} \tag{3.119}$$

Let us also define the essential infimum of effective travel delays

$$v_{ij} = \operatorname{essinf}\left[\Psi_p(t,h) : p \in \mathcal{P}_{ij}\right] \qquad \text{for all } \ (i,j) \in \mathcal{W}$$

The following definition of dynamic user equilibrium was first articulated by Friesz et al. (1993).

Definition 3.1. (Dynamic user equilibrium). *A vector of departure rates (path flows) $h^* \in \Lambda_0$ is a dynamic user equilibrium if*

$$h^*_p\left(t\right) > 0, p \in \mathcal{P}_{ij} \Longrightarrow \Psi_p\left[t, h^*\left(t\right)\right] = v_{ij}$$

We denote this equilibrium by $DUE\left(\Psi, \Lambda_0, [t_0, t_f]\right)$.

Using measure theoretic arguments, Friesz et al. (1993) established that a dynamic user equilibrium is equivalent to the following variational inequality under suitable regularity conditions:

$$\left.\begin{array}{c} \text{find } h^* \in \Lambda_0 \text{ such that} \\ \sum_{p\in\mathcal{P}} \int_{t_0}^{t_f} \Psi_p(t,h^*)(h_p - h_p^*)dt \geq 0 \\ \text{for all } h \in \Lambda_0 \end{array}\right\} VI(\Psi, \Lambda_0, [t_0, t_f]) \tag{3.120}$$

It has been noted in Friesz et al. (2011) that (3.120) is equivalent to a differential variational inequality. This is most easily seen by noting that the flow conservation constraints may be re-stated as

$$\left.\begin{array}{l} \dfrac{dy_{ij}}{dt} = \sum\limits_{p\in\mathcal{P}_{ij}} h_p(t) \\ y_{ij}(t_0) = 0 \\ y_{ij}(t_f) = Q_{ij} \end{array}\right\} \quad \text{for all } (i,j) \in \mathcal{W}$$

which is recognized as a two-point boundary value problem. As a consequence (3.120) may be expressed as the following differential variational inequality (DVI):

$$\left.\begin{array}{c} \text{find } h^* \in \Lambda \text{ such that} \\ \sum_{p\in\mathcal{P}} \int_{t_0}^{t_f} \Psi_p(t,h^*)(h_p - h_p^*)dt \geq 0 \\ \text{for all } h \in \Lambda \end{array}\right\} DVI(\Psi, \Lambda, [t_0, t_f]) \tag{3.121}$$

where

$$\Lambda = \left\{ h \geq 0 : \frac{dy_{ij}}{dt} = \sum_{p\in P_{ij}} h_p(t),\ y_{ij}(t_0) = 0,\ y_{ij}(t_f) = Q_{ij} \quad \text{for all } (i,j) \in \mathcal{W} \right\} \tag{3.122}$$

Finally, we are in a position to state a result that permits the solution of the DVI (3.121) to be obtained by solving a fixed-point problem:

Theorem 3.2. (Fixed point re-statement). *Assume that* $\Psi_p(\cdot, h) : [t_o,\, t_f] \longrightarrow \Re_+$ *is measurable for all* $p \in \mathcal{P}$, $h \in \Lambda$. *Then the fixed point problem*

$$h = P_\Lambda \left[h - \alpha \Psi(t, h) \right], \tag{3.123}$$

is equivalent to $DVI(\Psi, \Lambda, \Delta)$ *where* $P_\Lambda[\cdot]$ *is the minimum norm projection onto* Λ *and* $\alpha \in \Re_+$.

Proof. See Friesz (2010). □

3.3.2 The DNL subproblem

For the DNL sub-problem of the DUE model, we will employ the LWR-Lax model proposed by Friesz et al. (2012), which is a simplified version of the LWR model on networks. It is based on the assumption that any queues induced by congestion do not have physical size, thus no spillback occurs in the network. The network dynamics, including route and departure time choices, are summarized by a system of *differential algebraic equations* (DAEs). The derivation of the DAE system for DNL involves the variational method for Hamilton-Jacobi equations known as Lax-Hopf formula (Evans, 2010; Lax, 1957). For the brevity of our discussion, we will directly present the

DAE system describing and predicting the flow propagation as well as path delay. More detailed derivation of this DAE system can be found in Friesz et al. (2012).

Given a vehicular network $(\mathcal{A}, \mathcal{V})$, where $\mathcal{A}$ denotes the set of arcs, and $\mathcal{V}$ denotes the set of nodes, define for each arc $e \in \mathcal{A}$, the free flow speed v_0^e and the jam density ρ_{jam}^e. Assume that the arc dynamic is governed by the following conservation law

$$\partial_t \rho^e(t, x) + \partial_x f^e\big(\rho^e(t, x)\big) \;=\; 0 \tag{3.124}$$

where $\rho^e(t, x)$ is the vehicle density on the link e. The fundamental diagram $f^e(\cdot)$ is given as follows (Greenshields)

$$f^e(\rho) \;=\; v_0^e \, \rho \left(1 - \frac{\rho}{\rho_{jam}^e}\right) \tag{3.125}$$

We start by introducing some notations

$\mathcal{A}$: the set of all arcs

$\mathcal{V}$: the set of all nodes

$\mathcal{W}$: the set of all origin-destination pairs

$\mathcal{P}$: the set of utilized paths

$\mathcal{P}_{ij}$: the set of utilized paths that connects origin-destination pair $(i, j) \in \mathcal{W}$

$p \;=\; \{e_1, e_2, \ldots, e_{m(p)}\} \in \mathcal{P},\ e_i \in \mathcal{A}$: path represented by the set of arcs it uses

$h_p(t)$: departure rate at origin, associated with path p

$Q_p^e(t)$: entering vehicle count at arc e associated with path p

$q_p^e(t)$: enter rate at arc e associated with path p

$W_p^e(t)$: exiting vehicle count at arc e associated with path p

$w_p^e(t)$: exit rate at arc e associated with path p

L^e : length of arc $e \in \mathcal{A}$

ψ^e : the Legendre transformation of the following function

$$\phi(u) \;=\; \inf\big\{\rho \in [0, \rho_{jam}^e] : \;\; f^e(\rho) \;=\; u\big\}$$

where $f^e(\cdot)$ is the fundamental diagram associated with $e \in \mathcal{A}$

$D(t\,; Q^e)$: delay operator on arc e, associated with boundary profile Q^e

$$Q^e(t) \;\doteq\; \sum_{e \in p} Q_p^e(t), \quad W^{e_i}(t) \;\doteq\; \sum_{e_i \in p} W_p^{e_i}(t); \qquad i \geq 2$$

By convention, we write $q_p^{e_1}(t) \;=\; h_p(t),\ w_p^{e_0}(t) \;=\; h_p(t)$. The following DAE system (3.126)-(3.131)

for network loading was given in Friesz et al. (2012).

$$Q^e(t) \doteq \sum_{e\in p} Q_p^e(t), \quad q^e(t) \doteq \sum_{e\in p} q_p^e(t), \quad w^e(t) \doteq \sum_{e\in p} w_p^e(t) \tag{3.126}$$

$$\frac{d}{dt}Q_p^e(t) = q_p^e(t), \quad \frac{d}{dt}W^e(t) = w^e(t) \quad \text{for all } p\in\mathcal{P} \tag{3.127}$$

$$q_p^{e_i}(t) = w_p^{e_{i-1}}(t); \qquad i\in[1,\, m(p)],\ p\in\mathcal{P} \tag{3.128}$$

$$W^e(t) = \min_{\tau}\Big\{Q^e(\tau) + L^e\psi^e\Big(\frac{t-\tau}{L^e}\Big)\Big\}; \qquad \text{for all } e\in\mathcal{A} \tag{3.129}$$

$$Q^e(t) = W^e\big(t + D(t;\, Q^e)\big); \tag{3.130}$$

$$w_p^{e_i}\big(t + D(t;\, Q^{e_i})\big) = \frac{q_p^{e_i}(t)}{q^{e_i}(t)} w^{e_i}\big(t + D(t;\, Q^{e_i})\big); \qquad i\in[1,\, m(p)],\ p\in\mathcal{P} \tag{3.131}$$

We note that (3.126) is definitional, i.e. the traffic on an arc is disaggregated by different route choices. (3.128) represents the fundamental recursion, which allows the algorithm to carry forward to the next arc in the path. (3.129) is the Lax-Hopf formula (Bressan and Han, 2011a,b). (3.130) is often referred to as the flow propagation constraint, from which the travel time function $D(\cdot; Q^e)$ can be solved. (3.131) describes the diverging model satisfying first-in-first-out.

One shortcoming of the above DNL procedure is the lack of consideration for spillback, which not only aggravates congestion, but also causes a lot more stop-and-go waves (Colombo and Groli 2003) that will be another source of traffic emission. Thus as our next effort to model emission on a network level, we will consider the Lighthill-Whitham-Richards model on a network that captures spillover.

3.4 The DNL subproblem integrated with emission models

In this section, we will discuss two mesoscopic approaches for modeling traffic emission on a road network. The emission model will be considered in connection with the DNL sub-problem, which is consistent with established path flows as well as the flow propagation constraints. As a result, the output of the DNL sub-problem will include 1) the effective delay associated with each pair of departure time and route choices, and 2) the emission associated with each pair of departure time and route choices, as well as the total emission of the network.

3.4.1 Emission as a functional of velocity and acceleration

Consider a road network $(\mathcal{A},\, \mathcal{V})$. For each arc $a\in\mathcal{A}$, let us denote by $\rho_a(t,\, x)$, $v_a(t,\, x)$ the density and velocity of vehicles at time t and location x. The classical Lighthill-Whitham-Richards (LWR) model (Lighthill and Whitham 1955, Richards 1956) then describes the temporal-spatial evolution of $\rho_a(t,\, x)$ by

$$\frac{\partial}{\partial t}\rho_a(t,\, x) + \frac{\partial}{\partial x}\Big(\rho_a(t,\, x)\, v\big(\rho_a(t,\, x)\big)\Big) = 0 \tag{3.132}$$

where the velocity is expressed as an explicit function of density. The map $\rho \mapsto \rho\cdot v(\rho)$ is the fundamental diagram.

Following the modal emission model on a microscopic level (Barth et al. 1996), the rate of emission $e(t)$ of a moving vehicle can be modeled as a function of instantaneous velocity $v(t)$ and acceleration $a(t)$:

$$e(t) = \mathcal{E}\big(v(t),\, a(t)\big) \tag{3.133}$$

see Barth et al. (1996) for a detailed description of the function $\mathcal{E}$. The total emission associated with a particular vehicle is expressed as a functional of velocity and acceleration

$$\text{total emission} \;=\; \int_{t_0}^{t_f} \mathcal{E}\big(v(t),\, a(t)\big)\, dt$$

Consider an arc $a \in \mathcal{A}$ represented by a spatial interval $[0,\, L_a]$ and a solution $\rho_a(t,\, x)$, $v_a(t,\, x)$, $(t,\, x) \in [t_0,\, t_f] \times [0,\, L_a]$ to the LWR conservation law (3.132). Then the total emission on this arc is given by

$$\int_{t_0}^{t_f} \int_0^{L_a} \rho_a(t,\, x) \cdot e(t,\, x)\, dx\, dt \tag{3.134}$$

$$= \int_{t_0}^{t_f} \int_0^{L_a} \rho_a(t,\, x) \left(\mathcal{E} \left(v_a(t,\, x),\, \frac{D}{Dt}\, v_a(t,\, x) \right) \right) dx\, dt \tag{3.135}$$

$$= \int_{t_0}^{t_f} \int_0^{L_a} \rho_a(t,\, x) \left(\mathcal{E} \left(v_a,\, \frac{\partial}{\partial t} v_a + v_a \cdot \frac{\partial}{\partial x} v_a \right) \right) dx\, dt \tag{3.136}$$

where $\frac{D}{Dt} \doteq \frac{\partial}{\partial t} + v_a \cdot \frac{\partial}{\partial x}$ is the material derivative in Eulerian coordinates corresponding to the acceleration of the car in Lagrangian ones.

Notice that the formulation (3.136) can only be considered in the distributional sense, since the solutions ρ_a, v_a to the scalar conservation law are not differentiable. A detailed study of the continuous-time and discrete-time formulations of macroscopic emission models based on (3.136) is left as future research.

3.4.2 Emission as a functional of velocity

In this section, we will discuss the travel speed emission models, and integrate them with the DNL sub-problem in Section 3.3.2. The model is based on the average travel speed for an arbitrary period of time. Such models ignore certain granularity of the flow dynamics and are calibrated and validated by empirical data; see Rose et al. (1965), Kent and Mudfor (1979), and CARB (2000) for more discussion on velocity-based emission models. We assume that the average emission rate $\bar{e}(t)$ is a function of average velocity $\bar{v}(t)$:

$$\bar{e}(t) \;=\; \overline{\mathcal{E}}\big(\bar{v}(t)\big) \tag{3.137}$$

The speed $\bar{v}(t)$ can be averaged over a period that, say, spans a link traversal time. Given any feasible path flows $h \in \Lambda$, we can solve the DNL solution in a way proposed by Friesz et al. (2012). Let $D_p(t,\, h)$ denote the total traversal time for path p given that departure from the origin occurs at time t. In addition, we let $\tau^p_{a_i}(t)$ be the time of exit from arc a_i given that departure from the origin occurs at time t and path p is followed, where $p = \{a_1,\, \ldots,\, a_{m(p)}\}$. Then the average speed on the link a_i when the departure time from the origin occurs at t, denoted by $\bar{v}_{a_i}(t,\, h)$ is given by

$$\bar{v}_{a_i}(t,\, h) \;=\; \frac{L_{a_i}}{\tau^p_{a_i}(t) - \tau^p_{a_{i-1}}(t)}, \qquad t \in [t_0,\, t_f],\;\; p \in \mathcal{P}$$

where L_{a_i} is the length of arc $a_i \in p$. Then using equality (3.137), the contribution to emission of users departing at time t along path p is given by

$$E_p(t,\, h) \;\doteq\; \sum_{a_i \in p} \Big(\tau^p_{a_i}(t) - \tau^p_{a_{i-1}}(t) \Big) \cdot \bar{\mathcal{E}} \left(\frac{L_{a_i}}{\tau^p_{a_i}(t) - \tau^p_{a_{i-1}}(t)} \right) \tag{3.138}$$

Notice that we express the emission in a way similar to the effective delay operator $\Psi_p(t,\, h)$; such formulation will facilitate the derivation of gradient of the objective function in Section 3.6.

The total emission of the network associated with the path flow vector h is easily calculated as

$$\text{total emission} \;=\; \sum_{p\in\mathcal{P}} \int_{t_0}^{t_f} h_p(t)\cdot E_p(t,\, h)\, dt \tag{3.139}$$

Remark 3.3. *In Rose et al. (1965), Kent and Mudford (1979), and CARB (2000), it was the emission per unit distance e_x that was measured against travel speed, instead of emission per unit time e_t, see (3.115), (3.116), and (3.117). However, the emission per unit time as in (3.137) can be easily calculated as*

$$\bar{\mathcal{E}}\big(\bar{v}(t)\big) \;=\; \bar{e}(t) \;=\; \frac{\partial}{\partial t} e(t,\, x) \;=\; \frac{\partial x}{\partial t}\,\frac{\partial}{\partial x} e(t,\, x) \;=\; \bar{v}(t)\cdot e_x \tag{3.140}$$

where e_x is given by any one of (3.115), (3.116), or (3.117).

3.5 Multiobjective Toll Pricing

Most of the current MPEC-based Dynamic Traffic Assignment problems deal with a single objective. Lawphongpanich and Hearn (2004) studied the efficient tolls in a static network. Friesz et al. (2007) extended their work to consider dynamic congestion tolls, and Yao et al. (2012) further studied a dynamic congestion pricing problem with demand uncertainty. In these studies, it was assumed that the Stackelberg leader seeks to minimize just the network congestion. However, the problem of congestion pricing with an emission-related objective is more subtle. The difficulty arises from the paradox that the most environment-friendly driving condition turns out to be very inefficient in terms of travel time (CARB 2000). Therefore, one major challenge we must overcome in solving the proposed model is to resolve the potential conflict between transportation efficiency and emission. Therefore, we proceed to formulate our dynamic congestion pricing problem as a multiobjective program:

$$\min_{\mathcal{Y}} \mathcal{U} := \left[\int_{t_0}^{t_f} \sum_{p\in P} \Psi_p(t, h^*) h_p^*(t) dt, \quad \int_{t_0}^{t_f} \sum_{p\in P} E_p(t, h^*) h_p^*(t) dt\right] \tag{3.141}$$

subject to

$$\sum_{p\in P} \int_{t_0}^{t_f} (\Psi_p(t, h^*) + \delta_{a,p}\mathcal{Y}_a)(h_p^* - h_p) \le 0 \tag{3.142}$$

$$h \in \Lambda \tag{3.143}$$

$$\Lambda := \left\{ h \ge 0 : \frac{dy_{ij}}{dt} = \sum_{p\in P_{ij}} h_p(t)\,,\; y_{ij}(t_0) = 0,\; y_{ij}(t_f) = Q_{ij} \quad \text{for all } (i,j)\in\mathcal{W} \right\} \tag{3.144}$$

$$0 \le \mathcal{Y}_a \le Y_{UB} \quad \text{for all } a \in \mathcal{A} \tag{3.145}$$

where $\mathcal{Y} := (\mathcal{Y}_a : a \in \mathcal{A})$, the first term appearing on the right-hand side of (3.141) is the total effective delay, the second term is the total emission as given in (3.139), and where

$$\delta_{a,p} = \begin{cases} 1 & \text{if path } p \text{ traverse arc } a \\ 0 & \text{otherwise} \end{cases}$$

and $Y_{UB} \in \Re_+$ denotes the prescribed upper bound to the toll. Constraint (3.142) is a straightforward extension of the VI formulation of DUE, which takes into account the toll prices $\mathcal{Y}_a$. One crucial term in the formulation is the effective delay operator $\Psi(\cdot,\cdot) : \Lambda \to (\mathcal{L}[t_0, t_f])^{|\mathcal{P}|}_+$. The evaluation of such operator is referred to as the DNL procedure and is realized by solving the DAE system in Section 3.3.2. Therefore, the above program is further constrained by (3.126)-(3.131), and (3.138)-(3.139). Notice that in the program above, $\mathcal{U}$ is a vector of objective functions.

Definition 3.4. (Pareto Optimal) *For a multiobjective optimization problem of the form:*

$$\min F(x) = [F_1(x), F_2(x), ..., F_k(x)]^T$$

subject to

$$x \in X$$

a feasible solution $x^* \in X$, where X denotes the feasible region, is Pareto optimal if and only if there does not exist another solution, $x \in X$, such that $F(x) \leq F(x^*)$, and $F_i(x) < F_i(x^*)$ for at least one function.

A Pareto optimum requires that there are no other feasible solutions that improve at least one objective without deteriorating another. Seeking to attain a Pareto optimum, we employ a common approach called weighted sum method. Successful examples of such an approach can be found in Zadeh (1963) and Murata et al. (1996). Some new insights into the weighted sum scalarization can be found in Marler and Arora (2010).

3.6 Solution Methodology

The DVI can be reformulated as complementarity constraints as follows:

$$(\Psi_p(t, h^*) + \delta_{a,p}\mathcal{Y}_a - \mu_{ij}) \perp h^*_p \;\text{ for all } p \in \mathcal{P}_{ij},\; ij \in \mathcal{W} \tag{3.146}$$

$$\Psi_p(t, h^*) + \delta_{a,p}\mathcal{Y}_a - \mu_{ij} \geq 0 \;\text{ for all } p \in \mathcal{P}_{ij},\; ij \in \mathcal{W} \tag{3.147}$$

$$h^*_p \geq 0 \;\text{ for all } p \in \mathcal{P} \tag{3.148}$$

where $h^* \in \Lambda$. With complementarity constraints substituting the DVI in the MPEC model, we are able to obtain a single-level mathematical program consisting of the objective function (3.141) and (3.126)-(3.131), and (3.138)-(3.139). Since the complementarity constraints may not satisfy MFCQ (Rodrigues and Monteiro, 2006; and Izmailov and Solodov, 2004), we propose to apply a penalty method to handle these constraints. In Monteiro and Meira (2011) the quadratic penalty approach, sometimes called the sequential penalty technique, was tested numerically with positive results in solving an MPCC. Following the quadratic penalty method, we penalize the complementarity constraints and obtain an augmented objective function as:

$$\mathcal{U} := [U_1(h^*, \mathcal{Y}, \mu, M),\; U_2(h^*, \mathcal{Y}, \mu, M)] \tag{3.149}$$

where

$$U_1(h^*, \mathcal{Y}, \mu, M) := \sum_{ij \in \mathcal{W}} \sum_{p \in \mathcal{P}_{ij}} \int_{t_0}^{t_f} \Psi_p(t, h^*) h^*_p dt + \mathcal{Q}(h^*, \mathcal{Y}, \mu, M) \tag{3.150}$$

$$U_2(h^*, \mathcal{Y}, \mu, M) := \sum_{ij \in \mathcal{W}} \sum_{p \in \mathcal{P}_{ij}} \int_{t_0}^{t_f} E_p(t, h^*) h^*_p dt + \mathcal{Q}(h^*, \mathcal{Y}, \mu, M) \tag{3.151}$$

$$\mathcal{Q}(h^*, \mathcal{Y}, \mu, M) := M \sum_{ij \in \mathcal{W}} \sum_{p \in \mathcal{P}_{ij}} \int_{t_0}^{t_f} \left[(\Psi_p(t, h^*) + \delta_{a,p} \mathcal{Y}_a - \mu_{ij}) h_p^* \right]^2 dt$$
$$+ M \sum_{ij \in \mathcal{W}} \sum_{p \in \mathcal{P}_{ij}} \int_{t_0}^{t_f} \left[max \left\{ \mu_{ij} - \Psi_p(t, h^*) - \delta_{a,p} \mathcal{Y}_a, 0 \right\} \right]^2 dt \quad (3.152)$$

where $\mu := (\mu_{ij} : ij \in \mathcal{W})$, and M is a properly large number. In order to compute the above multiobjective problem, we use a simple but commonly-used weighted sum scalarization method:

$$S_u(h, \mathcal{Y}, \mu, M) = \alpha U_1(h^*, \mathcal{Y}, \mu, M) + \beta U_2(h^*, \mathcal{Y}, \mu, M) \quad (3.153)$$

where $\alpha, \beta \in \Re_+$ are weights for two objectives, respectively. For normalization, we further require that $\alpha + \beta = 1$. Then, the problem becomes a single-level single-objective problem. Such a problem is computed with the gradient projection method by Friesz (2010).

3.7 Numerical study

In this section, we will numerically illustrate the solutions to the MPEC problems as well as the effectiveness of the dynamic toll in mitigating both congestion and emission. Consider the network shown in Figure 9, which consists of six arcs and five nodes. There are two origin-destination pairs (1, 3), (2, 3), among which four and two paths are utilized, respectively.

$$p_1 = \{3, 6\}, \quad p_2 = \{1, 2, 6\}, \quad p_3 = \{1, 2, 4, 5\}, \quad p_4 = \{3, 4, 5\}, \quad p_5 = \{6\}, \quad p_6 = \{4, 5\}$$

Assume that arc 1 is tolled, and the upper-level decision variable of the MPEC problem is the dynamic toll price imposed on arc 1. The lower level is a DUE problem where drivers choose their departure time and route in order to minimize the total travel cost, including a toll price.

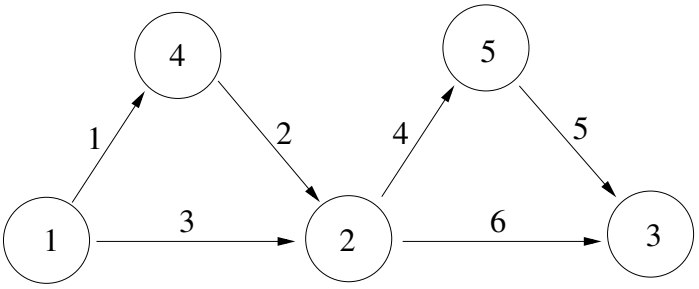

Figure 9: The 6 arc 5 node network

3.7.1 Numerical setting

We fix a morning commute horizon spanning five hours from 6:00 am to 11:00 am. The arc parameters are shown in Table 1.

We will employ the emission model discussed in Section 3.4.2 and Remark 3.3:

$$\bar{\mathcal{E}}\big(\bar{v}(t)\big) \;=\; \bar{v}(t) \cdot e_x$$

where the hot running emission e_x is given by (3.117):

$$e_x \;=\; \text{BER} \times \exp\left\{ b_1(v - 17.03) + b_2(v - 17.03)^2 \right\} \quad (3.154)$$

where BER $= 2.5$, $b_1 = -0.04$, $b_2 = 0.001$ (Smit 2006). We consider two cases in our computation:

Arc	Jam density (vehicle/mile)	Free flow speed (mile/hour)	Length (mile)
1	400	35	10
2	400	35	10
3	400	35	10
4	400	35	20
5	400	35	20
6	400	35	15

Table 6: Arc parameters for the network

I. The demand matrix is $(Q_{1,3}, Q_{2,3}) = (820, 410)$, and The upper bound for toll price is $Y_{UB} = 10$.

II. The demand matrix is $(Q_{1,3}, Q_{2,3}) = (1400, 700)$, and The upper bound for toll price is $Y_{UB} = 10$.

3.7.2 Numerical results

The solution algorithm for MPCC is implemented in Matlab (2010a), which runs on the Intel Xeon 3160 Dual-Core 3.0 GHz processor provided by the Penn State High Performance Computing Center.

Case I

We display the first numerical result from Case I above in Figures 12, 10, 11 and 13. For comparison reasons, we first solve the DUE problem without any tolls. The departure profiles at the beginning of each path are shown in Figure 10. Then the optimal solution to the MPEC problem which is a dynamic toll on arc 1, is presented in Figure 12. Under such toll price, the new equilibrium solution is now displayed in Figure 11. Notice that the two paths p_2, p_3 use link 1, and thus are affected by the toll. In the MPEC solution with toll, the path flows on p_2, p_3 diminish to the point where path p_3 is not used and very little traffic uses path p_2. Figure 13 shows the difference between the equilibrium path flows without toll, and the equilibrium path flows with optimal toll. It is clear that most of the users on path p_2, p_3 switch to path p_1, p_4, due to the presence of the toll.

We also compare the two objective functions in the case of DUE with toll and DUE without toll. The results are summarized in Table 2. It is clear that by adding the toll, we are able to reduce the total travel cost and total emission by 2.9% and 10.4%, respectively.

	Total travel cost	Total emission
DUE without toll	3.4744E+04	3.1789E+06
DUE with toll	3.3723E+04	2.8483E+06

Table 7: Comparison between DUE solutions. Case I.

Case II

In the Case II, the demand for each O-D pair is increased. The same quantities of the solution as in Case I are shown in Figures 14, 15, 16 and 17. Unlike the first case, in Case II there is very little difference of the DUE solutions with and without tolls. We interpret such results with the following intuition: when the demand increases, the system becomes less sensitive to control parameters,

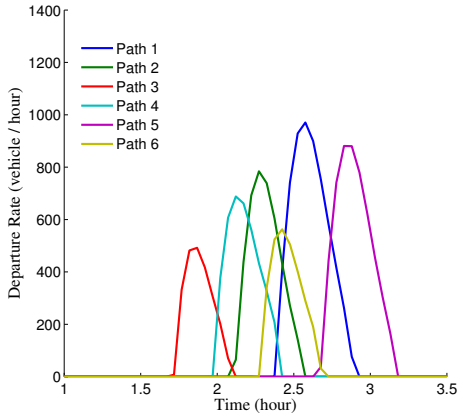

Figure 10: Case I. DUE solution without any toll

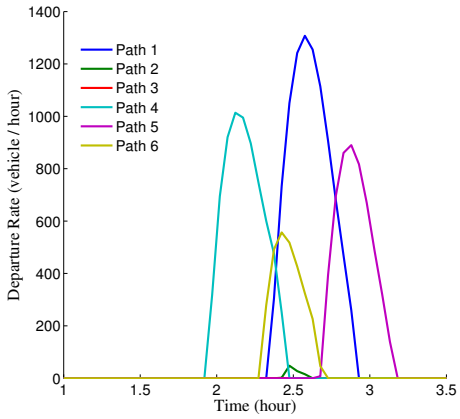

Figure 11: Case I. DUE solution with optimal toll.

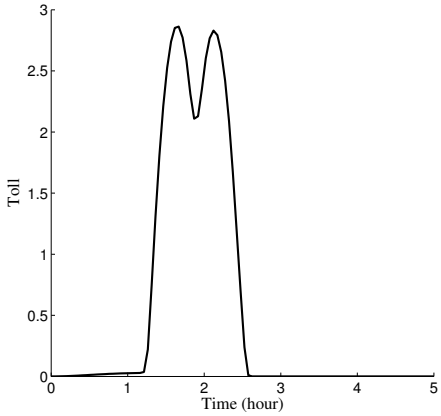

Figure 12: Case I. Optimal toll on arc 1.

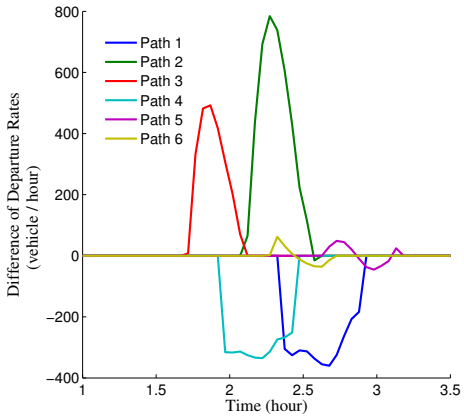

Figure 13: Case I. Differences of path flows between DUE without toll and DUE with toll.

making the system less controllable. This is also reflected from the comparison of objectives, as shown in Table 3. The reduction of total travel cost and total emission is only 0.04% and 0.45%.

	Total travel cost	Total emission
DUE without toll	7.5962E+04	5.4119E+06
DUE with toll	7.5932E+04	5.3878E+06

Table 8: Comparison between DUE solutions. Case II.

3.7.3 Different weights, the Braess's paradox

The multi-objective program is solved using the weighted sum scalarization method. We use different weights for total travel cost and total emission and see how the solution is affected. The test is conducted for Case I and Case II, the results are summarized in Table 4 and Table 5, respectively.

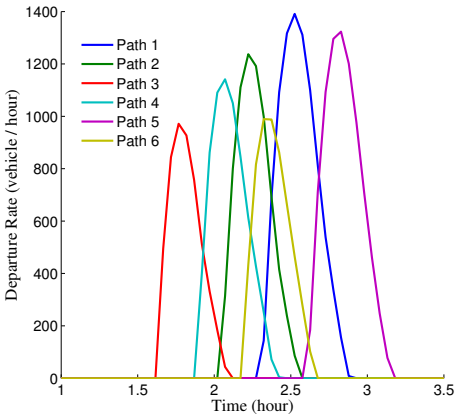

Figure 14: Case II. DUE solution without any toll.

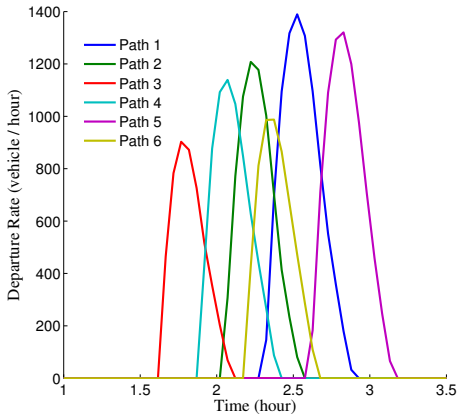

Figure 15: Case II. DUE solution with optimal toll.

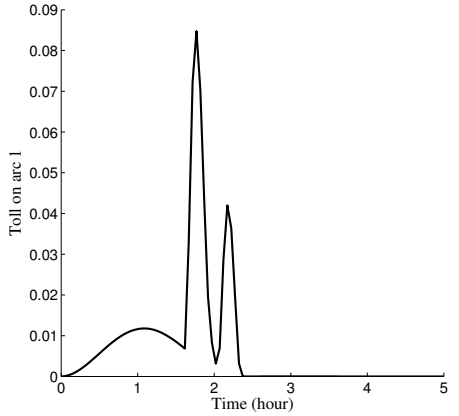

Figure 16: Case II. Optimal toll on arc 1.

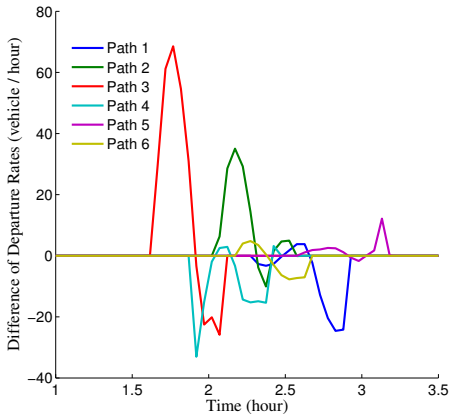

Figure 17: Case II. Differences of path flows between DUE without toll and DUE with toll.

We indicate by α the weight for the total travel time, by β the weight for the emission.

	Total travel cost	Total emission	α	β
Weight i,	3.3723E+04	2.8482E+06	0.0988	0.9011
Weight ii,	3.3723E+04	2.8483E+06	0.9434	0.0566

Table 9: Comparison of objectives for different choices of weights, Case I. α is the weight of total travel cost, β is the weight of total emission.

Another interesting phenomenon is the Braess-like paradox displayed in Case I, where the performance of the network, whether in terms of travel cost or emission, is enhanced in the more constrained system (the one with toll).

	Total travel cost	Total emission	α	β
Weight i,	7.5932E+04	5.3878E+06	0.0138	0.9862
Weight ii,	7.8360E+04	5.2396E+06	0	1
Weight iii,	7.5858E+04	5.4175E+06	1	0

Table 10: Comparison of objectives for different choices of weights, Case II. α is the weight of total travel cost, β is the weight of total emission.

3.7.4 Discussions

In the numerical tests, we solved two cases of a simple network. The results provide some interesting phenomena and interpretations to our proposed model and the dynamic toll pricing problem in general.

First, as noted above, the optimal toll creates a Braess-like paradox in Case I. A Braess' paradox (Braess 1969) states that the system's overall performance can be reduced in some cases with added extra capacity when traffic agents selfishly decide their route. In our problem setting, the traffic agents all choose both their route and departure time that appear most favorable to themselves. By imposing the toll, affordable time windows on path p_2 and path p_3 become significantly smaller. In particular, we notice that in the presence of the toll, the path p_3 is completely abandoned by the users. With fewer affordable choices on path and/or departure time, the system's capacity becomes more constrained, yet two measures of the system performance, the total traffic cost and the overall emission amount, are reduced, i.e. a higher efficiency is attained in terms of both transportation and environment.

Second, tolls can act as effective stimuli in a transportation system. We observe from Table 2 (in Case I) and Table 3 (in Case II) that by properly choosing the toll prices, one can reduce both the total traffic cost and total emission. In Case I, the price of toll on the first arc of path p_2 renders this path no longer an affordable choice, i.e. the equilibrium flow on this path vanishes, which, nonetheless, creates a Braess-like paradox as discussed above.

Finally, by comparing Table 4 and Table 5, in response to changing weights for the two objectives in our weighted sum approach, Case I (in Table 4) shows very minor changes in objective values compared to Case II (in Table 5). The reason for such a difference in the sensitivity to weight perturbations is still a point of research curiosity. Nonetheless, this points to the necessity of a careful determination of weights for the two objectives in our model in order to attain the optimization goal of the central control.

3.8 Conclusion

This project proposes a congestion pricing problem that takes into account the environmental impact of traffic dynamics on a vehicular network. An MPEC problem is formulated which aims at mitigating both emission and congestion on a network level. For the vehicle-induced emissions, we employ a mesoscopic modeling approach, which uses macroscopic traffic quantities and microscopic emission functions. The emission model is then embedded in the dynamic network loading subproblem of DUE in the following way: for every given set of departure rates at the origin, we run the network loading procedure until all macroscopic traffic quantities are available; then we provide vehicle dynamics information to the microscopic emission function and perform emission estimation on a network-wide level. The MPEC problem is first reformulated as an MPCC. To avoid violation of constraint qualifications, we then apply a quadratic penalty-based method to relax the original program. The relaxed model is solved with the gradient projection algorithm (Friesz 2010) with mul-

tiobjective handled via a weighted sum scalarization. The numerical examples have demonstrated the effectiveness of congestion toll in controlling and reducing both total travel cost and emission. We also observe an instance of the Braess-like paradox where a more constrained system results in higher transportation efficiency and less environmental impact.

The emission model employs the average velocity-based emission function (CARB 2000). Such a model is computationally convenient in terms of integration with the DNL procedure. However, it relies on the average speed of cars, and therefore is less accurate compared to other models that depend on instantaneous speed and acceleration. As our future research, we will take into account spill-over into our DNL model and capture the speed variation in a more accurate way.

Kumar and Vladimirsky (2010) pointed out that a weighted sum scalarization approach could obtain only the convex part of the Pareto front, which might lead to selecting suboptimal trajectories. To resolve such an issue, they provided an alternative "marching" method. The application of their approach to our model is also of our future research interest.

4 Outcomes of the Project

As the outcomes of the project, several projects have been accepted and disseminated in journals and selective transportation research conferences, including International Symposium on Transportation and Traffic Theory (ISTTT) and Triennial Symposium on Transportation Analysis (TRISTAN). Specifically, the detailed information on these projects are given as follows:

- Friesz, T.L., Han, K., Liu, H., Yao, T., 2013. Dynamic congestion and tolls with mobile source emission. In *Proceedings of the 20th International Symposium on Transportation and Traffic Theory* (ISTTT 2013). The Netherlands, 17-19 July 2013.

- Friesz, T.L., Han, K., Liu, H., Yao, T., 2013. Dynamic congestion and tolls with mobile source emission. *Procedia - Social and Behavioral Sciences*, 80, 818-836.

- Han, K., Friesz, T.L., Liu, H., Yao, T., 2012. A robust optimization approach for dynamic traffic signal control with emission constraints. Project accepted for presentation at the Eighth Triennial Symposium on Transportation Analysis (TRISTAN VIII).

In addition, some conference presentations to disseminate the findings of the project are listed as following:

- Han, K., Friesz, T.L., Liu, H., Yao, T., 2013. A Robust Optimization Approach for Adaptive Traffic Signal Control with Emission Constraints. *INFORMS Annual Meeting 2013*.

- Han, K., Sun, Y. Liu, H., Friesz, T.L., Yao, T., 2013. A bi-level model of dynamic traffic signal control with continuum approximation. *INFORMS Annual Meeting 2013*.

5 Impact of the Project

This project provides a spectrum of new models and substantially extends the current literature in addressing traffic control and congestion/emission mitigation with potential incorporation of realistic data.

The research findings, made public in the forms of publications and conference presentations, can potentially impact multiple disciplines including civil engineering, operations management, operations research, optimization, and transportation. In practice, the proposed formulations and solution schemes can aid traffic network designers / managers in making non-trivial planning decisions.

References

Anitescu, M. (2000). On solving mathematical programs with complementarity constraints as nonlinear programs. *Preprint ANL/MCS-P864-1200*, MCS Division, Argonne National Laboratory, Argonne, IL.

Arnott, A., de Palma, A., & Lindsey, R. (1990). Departure time and route choice for the morning commute. *Transportation Research Part B*, 24(3), 209-228.

Arnott, R., & Kraus, M. (1998). When are anonymous congestion charges consistent with marginal cost pricing? *Journal of Public Economics*, 67(1), 45-64.

Arnott, R., & Small, K. (1994). The economics of traffic congestion. *American Scientist*, 82(5), 446-455.

Atamtürk, A., Zhang, M., 2007. Two-stage robust network flow and design under demand uncertainty. Operations Research 55 (4), 662-673.

Aubin, J.P., Bayen, A.M., Saint-Pierre, P., 2008. Dirichlet problems for some Hamilton-Jacobi equations with inequality constraints. SIAM Journal on Control and Optimization 47 (5), 2348-2380.

Aziz, H.M.A. and Ukkusuri, S.V. 2012. Integration fo environmental objectives in a system optimal dynamic traffic assignment model. Computer-Aided Civil and Infrastructure Engineering 27, 494-511.

Ban, J.X., Liu, H.X., Ferris, M.C., & Ran, B. (2006). A general MPCC model and its solution algorithm for continuous network design problem. *Mathematical and Computer Modeling*, 43, 493-505.

Barth, M., An, F., Norbeck, J., Ross, M. (1996). Modal emission modeling: A physical approach. *Transportation Research Record*, 1520, 81-88.

Braess, D. (1969). Über ein Paradoxon aus der Verkehrsplanung. *Unternehmensforschung*, 12, 258-268.

Braid, R. (1996). Peak-load pricing of a transportation route with an unpriced substitute. *Journal of Urban Economics*, 40(2), 179-197.

Bressan, A., & Han, K. (2011). Optima and Equilibria for a model of traffic flow. *SIAM Journal on Mathematical Analysis*, 43(5), 2384-2417.

Bressan, A., & Han, K. (2011). Nash Equilibria for a Model of Traffic Flow with Several Groups of Drivers. *ESAIM: Control, Optimization and Calculus of Variations*, 18(4), 969-986.

Bandi, C., D. Bertsimas. 2012. Tractable stochastic analysis in high dimensions via robust optimization. Mathematical Programming, Series B. DOI: 10.1007/s10107-012-0567-2

Barnhart, C., Johnson, E.L., Nemhauser, G.L., Savelsbergh, M.W.P., Vance, P.H., 1998. Branch-and-price: column generation for solving huge integer programs. Operations Research 46(3), 316-239.

Barth, M., An, F., Norbeck, J., Ross, M., (1996). Modal emission modeling: a physical approach. Transportation Research Record 1520, 81-88.

Ben-Tal, A., A. Nemirovski. 1998. Robust convex optimization. Mathematics of Operations Research 23(4) 769–805.

Ben-Tal, A., A. Nemirovski. 1999. Robust solutions of uncertain linear programs. Operations Research Letters 25(1) 1–14.

Ben-Tal, A., A. Nemirovski. 2000. Robust solutions of linear programming problems contaminated with uncertain data. Mathematical Programming 88 411-421.

Benedek, C.M., Rilett, L.R., 1998. Equitable traffic assignment with environmental cost function. Journal of Transportation Engineering, 124, 16-22.

Bertsimas, D., D.B. Brown, C. Caramanis. 2011a. Theory and applications of robust optimization. SIAM Review 53(3) 464-501.

Bertsimas, D., Chang, A., Rudin, C., 2011. Integer optimization methods for supervised ranking. Available online at http://hdl.handle.net/1721.1/67362.

Bertsimas, D., Gamarnik, D., Rikun, A.A., 2011b. Performance analysis of queueing networks via robust optimization. Operations Research 59(2) 455-466.

Bertsimas, D., Gupta, V., Kallus, N., 2014. Data-driven robust optimization. Working project. Online at http://www.mit.edu/$\tilde{\text{v}}$gupta1/projects/DataDrivenRobOptv1.pdf

Bertsimas, D., M. Sim. 2004. Price of robustness. Operations Research 52(1) 35–53.

Bressan, A., 2000. Hyperbolic Systems of Conservation Laws.The One Dimensional Cauchy Problem. Oxford University Press.

Bretti, G., Natalini, R., Piccoli, B., 2006. Numerical approximations of a traffic flow model on networks, Networks and Heterogeneous Media 1, 57-84.

Burer, S., Letchford, A.N., 2012. Non-convex mixed-integer nonlinear programming: a survey. Surveys in Operations Research and Management Science 17, 97-106.

CARB (2000). Public Meeting to Consider Approval of Revisions to the States On-Road Motor Vehicle Emissions Inventory Technical Support Document. California Air Resources Board. May 2000.

Colombo, R.M., Groli, A., 2003. Minimizing stop and go waves to optimise traffic flow. *Applied Mathematics Letters*, 17, 697-701.

Christofa, E., Papmichail, I. and Skabardonis, A. 2013. Person-based traffic responsive signal control optimization. IEEE Transactions on Intelligent Transportation Systems, 14 (3), 1278-1289.

Claudel, C.G., Bayen, A.M., 2010. Lax-Hopf Based Incorporation of Internal Boundary Conditions Into Hamilton-Jacobi Equation. Part I: Theory. IEEE Transactions on Automatic Control 55 (5), 1142-1157.

Coclite, G.M., Garavello, M., Piccoli, B., 2005. Traffic flow on a road network. SIAM Journal on Mathematical Analysis 36 (6), 1862-1886.

Daganzo, C.F., 1994. The cell transmission model. Part I: A simple dynamic representation of highway traffic. Transportation Research Part B 28 (4), 269-287.

Daganzo, C.F., 1995. The cell transmission model. Part II: Network traffic. Transportation Research Part B 29 (2), 79-93.

Daganzo, C.F., 2005. A variational formulation of kinematic waves: basic theory and complex boundary conditions. Transportation Research Part B 39 (2), 187-196.

Daganzo, C.F., 2006. On the variational theory of traffic flow: well-posedness, duality and application. Network and heterogeneous media 1 (4), 601-619.

Daganzo, C.F. (1994). The cell transmission model. Part I: A simple dynamic representation of highway traffic. *Transportation Research Part B*, 28(4), 269-287.

Daganzo, C.F. (1995). The cell transmission model. Part II: Network traffic. *Transportation Research Part B*, 29(2), 79-93.

De Palma, A., & Lindsey, R. (2000). Private toll road: Competition under various ownership regimes. *The Annals of Regional Sciences*, 34(1), 13-35.

Dial, R. (1999). Minimum revenue congestion pricing Part I: A fast algorithm for the single-origin case. *Transportation Research Part B*, 33(3), 189-202.

Dial, R. (2000). Minimum revenue congestion pricing Part II: A fast algorithm for the general case. *Transportation Research Part B* 34(8), 645-665.

Evans, L.C., 2010. Partial Differential Equations. Second edition. American Mathematical Society, Providence, RI.

Ekström, M., Sjodin, A., & Andreasson, K. (2004). Evaluation of the COPERT III emission model within on-road. *Atmospheric Environment*, 38, 6631-6641.

Evans, L.C. (2010). *Partial Differential Equations*. Second edition. American Mathematical Society, Providence, RI.

Ferrari, P., 1995. Road pricing and network equilibrium. Transportation Research Part B 29 (5), 357-372.

Garavello, M., Piccoli, B., 2006. Traffic Flow on Networks. Conservation Laws Models. AIMS Series on Applied Mathematics, Springfield, Mo..

Gartner, N.H., 1983. OPAC: a demand-responsive strategy for traffic signal control. Transportation Research Record 906, 75-81.

Geoffrion, A.M., Marsten, R.E., 1972. Integer programming algorithms: a framework and state-of-the-art survey. Management Science 18(9), 465-491.

Godunov, S.K., 1959. A difference scheme for numerical solution of discontinuous solution of hydrodynamic equations. Math Sbornik 47 (3), 271-306.

Han, K., Friesz, T.L., Yao, T., 2013. A partial differential equation formulation of Vickrey's bottleneck model, part II: Numerical analysis and computation. Transportation Research Part B 49, 75-93.

Han, K., Friesz, T.L., Yao, T., 2014a. A variational approach for continuous supply chain networks. SIAM Journal on Control and Optimization 52(1), 663-686.

Han, K., Gayah, V., Piccoli, B., Friesz, T.L., Yao, T., 2014. On the continuum approximation of the on-and-off signal control on dynamic traffic networks. Transportation Research Part B: Methodological, 61, 73-97.

Friesz, T.L. (2010). *Dynamic Optimization and Differential Games*. Springer, New York.

Friesz, T.L., Bernstein, D., Smith, T., Tobin, R., & Wie, B. (1993). A variational inequality formulation of the dynamic network user equilibrium problem. *Operations Research*, 41(1), 80-91.

Friesz, T.L., Bernstein, D., Suo, Z., & Tobin, R.L. (2001). Dynamic network user equilibrium with state-dependent time lags. *Networks and Spatial Economics*, 1(3-4), 319-347.

Friesz, T.L., & Mookherjee, R. (2006). Solving the dynamic network user equilibrium problem with state-dependent time shifts. *Transportation Research Part B*, 40(3), 207-229.

Friesz, T.L., Kwon, C., & Mookherjee, R. (2007). A computable theory of dynamic congestion pricing. *Transportation and Traffic Theory 2007*, 1-26.

Friesz, T.L., Kim, T., Kwon, C., & Rigdon, M.A. (2011). Approximate network loading and dual-time-scale dynamic user equilibrium. *Transportation Research Part B*, 45(1), 176-207.

Friesz, T.L., Han, K., Neto, P.A., Meimand, A., & Yao, T. (2013). Dynamic user equilibrium based on a hydrodynamic model. *Transportation Research Part B*, 47(1), 102-126.

Han, K., Piccoli, B., Friesz, T.L., Yao, T., 2012. A continuous-time link-based kinematic wave model for dynamic traffic networks. arXiv: 1208.5141v1.

Hearn, D.W., & Ramana, M.V. (1998). Solving congestion toll pricing models. *In: Equilibrium and Advanced Transportation Modeling*, P. Marcotte, S. Nguyen (eds.), Kluwer Academic Publishers, Boston, pp. 109-124.

Herty, M., Klar, A., 2003. Modeling, simulation, and optimization of traffic flow networks, SIAM Journal on Scientific Computing 25 (3), 1066-1087.

Holden, H., Risebro, N.H., 1995. A mathematical model of traffic flow on a network of unidirectional roads, SIAM Journal on Mathematical Analysis 26 (4), 999-1017.

Hunt, P.B., Robertson, D.I., Bretherton, R.D., Royle, M.C., 1982. The scoot on-line traffic signal optimisation technique. Traffic Engineering and Control 23 (4), 190-192.

Improta, G., Cantarella, G.E., 1984. Control system design for an individual signalized junction. Transportation Research Part B 18 (2), 147-167.

]Izmailov, A. F., & Solodov, M. V. (2004). Newton-type methods for optimiztion problems without constraint qualifications. *SIAM Journal on Optimization*, 15(1), 210-228.

Jin, W.-L., 2010. Continuous kinematic wave models of merging traffic flow. Transportation Research Part B 44, 1084-1103.

Jin, W.-L., Zhang, H.M., 2003. On the distribution schemes for determining flows through a merge. Transportation Research Part B 37 (6), 521-540.

Kent, J.H. & Mudford, N.R. (1979). Motor vehicle emissions and fuel consumption modeling. *Transportation Research Part A*, 13(6), 395-406.

Kumar, A., & Vladimirsky, A. (2010). An efficient method for multi-objective optimal control and optimal control subject to integral constraints. *Journal of Computational Mathematics*, 28(4), 517-551.

Lax, P.D., 1957. Hyperbolic systems of conservation laws II. Communications on Pure and Applied Mathematics 10 (4), 537-566.

Lax, P.D., 1973. Hyperbolic systems of conservation laws and the mathematical theory of shock waves, SIAM.

Lebacque, J., Khoshyaran, M., 1999. Modeling vehicular traffic flow on networks using macroscopic models, in Finite Volumes for Complex Applications II, 551-558, Hermes Science Publications, Paris.

Lebacque, J., Khoshyaran, M., 2002. First order macroscopic traffic flow models for networks in the context of dynamic assignment, Transportation Planning State of the Art, M. Patriksson and K. A. P. M. Labbe, eds., Kluwer Academic Publushers, Norwell, MA.

LeVeque, R.J., 1992. Numerical Methods for Conservation Laws. Birkhäuser.

Li, C. and Shimamoto, S. 2011. Dynamic traffic light control scheme for reducing CO_2 emissions employing ETC technology. International Journal of Managing Public Sector Information and Communication Technologies 2 (1), 1-12.

Lighthill, M., Whitham, G., 1955. On kinematic waves. II. A theory of traffic flow on long crowded roads. Proceedings of the Royal Society of London. Series A, Mathematical and Physical Sciences 229 (1178), 317-345.

Lin, S., De Schutter, B., Zegeye, S.K., Hellendoorn, H. and Xi, Y. 2010. Integrated urban traffic control for the reduction of travel delays and emissions. Proceedings of the 13th International IEEE Conference on Intelligent Transportation Systems.

Lin, W.H., Wang, C., 2004. An enhanced 0 - 1 mixed-integer LP formulation for traffic signal control. IEEE Transactions on Intelligent transportation systems 5 (4), 238-245.

Lo, H., 1999. A novel traffic signal control formulation. Transportation Research Part A 33, 433-448.

Lo, H., 1999. A cell-based traffic control formulation: strategies and benefits of dynamic timing plans. Transportation Science 35 (2), 148-164.

Lo, H., A dynamic traffic assignment formulation that encapsulates the cell-transmission model. Transportation and Traffic Theory, 327-350.

Lv, J., Zhang, Y. and Zietsman, J. 2013. Investigating emission reduction benefit from intersection signal optimization. Journal of Intelligent Transportation Systems: Technology, Planning, and Operations 17 (3), 200-209.

Lawphongpanich, S., & Hearn, D. (2004). An MPEC approach to second-best toll pricing. *Mathematical Programming*, 101(1), 33-55.

Lax, P.D. (1957). Hyperbolic systems of conservation laws II. *Communications on Pure and Applied Mathematics*, 10(4), 537566.

Lighthill, M., & Whitham, G. (1955). On kinematic waves. II. A theory of traffic flow on long crowded roads. *Proceedings of the Royal Society of London: Series A*, 229, 317- 345.

Marler, R.T, & Arora, J.S. (2010). The weighted sum method for multi-objective optimization: new insights. *Structural and Multidisciplinary Optimization*, 41(6), 853-862.

Monteiro, M.T.T., & Meira, J.F.P. (2011). A penalty method and a regularization strategy to solve MPCC. *International Journal of Computer Mathematics*, 88(1), 145-149.

Murata, T., Ishibuchi, H., & Tanaka, H. (1996). Multi-objective genetic algorithm and its applications to flowshop scheduling. *Computers and Industrial Engineering*, 30(4), 957-968.

Moskowitz, K., 1965. Discussion of 'freeway level of service as influenced by volume and capacity characteristics' by D.R. Drew and C.J. Keese. Highway Research Record, 99, 43-44.

Nagurney, A. (1993). *Network economics: A variational inequality approach*. Kluwer Academic Publishers, Norwell, Massachusetts.

Nagurney, A., Qiang, Q., Nagurney, L.S., 2010. Environmental impact assessment of transportation networks with degradable links in an era of climate change. International Journal of Sustainable Transportation, 4, 154-171.

Newell, G.F., 1993. A simplified theory of kinematic waves in highway traffic, part I: General theory. Transportation Research Part B 27 (4), 281-287.

Mirchandani, P., Head, L., 2000. A real-time traffic signal control system: architecture, algorithms, and analysis. Transportation Research Part C 9, 415-432.

Penic, M. A., and J. Upchurch. TRANSYT-7F, Enhancement for Fuel Consumption, Pollution Emissions, and User Costs. In Transportation Research Record 1360, TRB, National Research Council, Washington, D.C., 1992.

Post, K., Kent, J.H., Tomlin, J., Carruthers, N., 1984. Fuel consumption and emission modelling by power demand and a comparison with other models. Transportation Research Part A 18 (3), 191-213.

Panis, L.I., Broekx, S., & Liu, R. (2006). Modeling instantaneous traffic emission and the influence of traffic speed limits. *Science of the Total Environment*, 371, 270-285.

Pareto, V. (1906). *Manuale di Economica Politica, Societa Editrice Libraria*. Milan; translated into English by A.S. Schwier as *Manual of Political Economy*, edited by A.S. Schwier and A.N. Page, 1971. New York: A.M. Kelly.

Pigou, A. (1920). *The economics of welfare*. London: Macmillan and Co.

Robertson, D.I., Lucas, C.F. and Baker, R.T. 1980. Coordinating traffic signals to reduce fuel consumption. TRL Report LR934. Transport Research Laboratory, Crowthorne, Berkshire, United Kingdom.

Richards, P.I., 1956. Shockwaves on the highway. Operations Research 4 (1), 42-51.

Rikun, A.A. 2011. Application of robust optimization to queueing and inventory systems. Ph.D. Dissertation. Sloan School of Management. Massachusetts Institute of Technology.

Raghunathan, A.U., Diaz, M.S.,& Biegler, L.T. (2004). An MPEC formulation for dynamic optimization of distillation operations. *Computers and Chemical Engineering*, 28, 2037-2052.

Rakha, H., Ahn, K., & Trani, A. (2004). Development of VT-Micro model for estimation hot stabilized light duty vehicle and truck emissions. *Transportation Research Part D*, 9(1), 49-74.

Ralph, D., & Wright, S.J. (2004). Some properties of regularization and penalization schemes for MPECs. *Optimization Methods and Software*, 19, 527-556.

Richards, P.I., 1956. Shockwaves on the highway. *Operations Research*, 4(1), 42-51.

Rodrigues, H.S., & Monteiro, M.T.T. (2006). Solving mathematical programs with complementarity constraints with nonlinear solvers. *Recent Advances in Optimization. Lecture Notes in Economics and Mathematical Systems,* 563(IV), 415-424.

Rose, A.H., Smith, R., McMichael, W.F. & Kruse, R.F. (1965) Comparison of auto exhaust emissions in two major cities. *Journal of the Air Pollution Control Association*, 15(8), 362-371.

Shen, W., Nie, Y., Zhang, H.M., 2007. Dynamic network simplex method for designing emergency evacuation plans. Trans. Res. Rec. No. 2022, 83-93.

Smit, R. (2006). An examination of congestion in road traffic emission models and their application to urban road networks. Ph.D. thesis, Griffith University.

Sims, A.G., Dobinson, K.W., 1980. The Sydney coordinated adaptive traffic (SCAT) system philosophy and benefits. IEEE Transactions on Vehicular Technology 29 (2), 130-137.

Skabardonis, A., 2000. Control strategies for transit priority. Transportation Research Record: Journal of the Transportation Research Board, No. 1727, TRB, National Research Council, Washington, D.C., 2000, pp. 20-26.

Stevanovic, A., Stevanovic, J., Zhang, K. and Batterman, S. 2009. Optimizing traffic control to reduce fuel consumption and vehicular emissions: Integrated approach with VISSIM, CMEM, and VISGAOST. Transportation Research Record 2128, 105-113.

Szeto, W.Y., Jaber, X., Wong, S.C., 2012. Road network equilibrium approaches to environmental sustainability. Transport Reviews: A Transnational Transdisciplinary Journal 32 (4), 491-518.

Wismans, L. (2012). Towards sustainable dynamic traffic management. Ph.D. Dissertation. University of Twente, Faculty of Engineering Technology, Center for Transport Studies.

Yang, H., & Huang, H.J. 2005. *Mathematical and Economic Theory of Road Pricing*. Elsevier Oxford.

Yao, T., Friesz, T.L., Chung, B.D., Liu, H. 2012. Dynamic congestion pricing under uncertainty: a robust optimization approach. *Transportation Research Part B*, 46(10), 1504-1518.

Yang, H., Bell, M.G.H, 1997. Traffic restraint, road pricing and network equilibrium. Transportation Research Part B 31, 303-314.

Yang, H., Xu, W., He, B., Meng, Q., 2010. Road pricing for congestion control with unknown demand and cost functions. Transportation Research Part C 18, 157-175.

Yperman, I., S. Logghe and L. Immers, 2005. The Link Transmission Model: An Efficient Implementation of the Kinematic Wave Theory in Traffic Networks, Advanced OR and AI Methods in Transportation, Proc. 10th EWGT Meeting and 16th Mini-EURO Conference, Poznan, Poland, 122-127, Publishing House of Poznan University of Technology.

Zhang, L., Yin, Y. and Chen, S. 2013. Robust signal timing optimization with environmental concerns. Transportation Research Part C 29, 55-71.

Zadeh, L.A. (1963). Optimality and non-scalar-valued performance criteria. *IEEE Transactions on Automatic Control* AC-8, 5960

Zegeye, S.K., Schutter, B., Hellendoorn, J., Breunesse, E.A. (2010). Integrated macroscopic traffic flow and emission model based on METANET and VT- micro. *Proceedings of the International Conference on Models and Technologies for Intelligent Transportation Systems*, Rome, Italy, June 2009 (G. Fusco, ed.), Rome, Italy: Aracne Editrice, ISBN 978-88-548-3025-7, 8689.